Townsend, K.T., Nelson, M.S., Rittenour, T.M., and Pederson, J.L., 2019, Anatomy and evolution of a dynamic arroyo system, Kanab Creek, southern Utah, USA: Geological Society of America Bulletin.

https://doi.org/10.1130/B35195.1

DATA REPOSITORY Item 2019168

TABLE OF CONTENTS

SUPPLEMENTAL METHODS

Longitudinal Profile Concavity

Concavity and steepness indexes along drainages are ultimately derived from the stream power incision model (e.g. Howard and Kerby, 1983; Whipple and Tucker, 1999). Then, assuming a river profile is in steady state with respect to climate, uplift, and substrate conditions, it can be simplified to a power-law expression, known as Flint's Law, relating stream gradient to contributing drainage area as a proxy for discharge:

$$S = k_s A^{-\theta}$$

where S is local channel gradient, A is upstream drainage area, and k_s and Θ are the steepness and concavity indices, respectively (Howard and Kerby, 1983). Both k_s and Θ can be determined through regression of river gradient and contributing area data, where Θ is the slope of the regression line and k_s is the y-intercept.

Optically Stimulated Luminescence (OSL) Dating

Age control for allostratigraphic alluvial sequences was obtained using a combination of AMS radiocarbon dating of charcoal (n = 47) and optically stimulated luminescence (OSL) dating of quartz sand (n = 54). In depositional settings, OSL dating provides an age estimate of the last time sediment was exposed to light (Huntley et al. 1985). Following deposition and burial, the luminescence signal accumulates in quartz and feldspar minerals over time due to exposure to ionizing radiation from the surrounding sediments (radio-isotopes of Potassium, Uranium, Thorium and Rubidium). The accumulated luminescence signal measured in a sample is directly proportional to the radioactivity of the surrounding sediments (environmental dose rate, D_R, measured in units of Grays per thousand years, Gy/ka, where 1 Gy= 1 Joule/kg) and the length of time since the sample was last exposed to light (burial age, measured as the equivalent dose, D_E, of radiation needed to induce a luminescence signal similar to that obtained during burial). Luminescence ages are calculated by:

$$\text{Age} = \frac{\text{equivalent dose } (D_E), \text{ Gy}}{\text{dose rate } (D_R), \text{ Gy/ka}}$$

Samples for OSL dating were collected by pounding opaque metal tubes into selected sandy horizons and extraction of the light-safe interior portions of the tubes for dating. Plane-bedded and ripple cross-bedded sandy horizons were preferentially targeted to help reduced influence of partial bleaching (incomplete resetting) of the luminescence signals following suggestions of Summa-Nelson and Rittenour (2012). Representative sediment within 30 cm of each tube was collected for dose rate determination. Samples were sealed and brought to the Utah State University Luminescence Lab for processing and analysis.

Samples were opened under dim amber laboratory lighting (~590 nm) and the outer 2cm of sediment at the ends of the tubes was removed. The fine-grained quartz sand fraction was purified from the inner (light-safe) portion of the sample tubes for dating. Sediment was wet-sieved to specific grain-size fractions (generally 150-250 µm or 180-250 µm), and subsequently pretreated with 10% hydrochloric acid to dissolve carbonates and chlorine bleach to remove organic material. A heavy mineral separation was performed using sodium polytungstate (2.7 g/cm^3), followed by three concentrated hydrofluoric acid treatments (30 minutes each) to remove feldspars and etch quartz grains. Concentrated hydrochloric acid was then used to remove any precipitated fluorites.

The single-aliquot regenerative-dose (SAR) technique of Murray and Wintle (2000) was used for OSL dating of single-grains and small-aliquots (2 mm diameter, ~10-60 grains per disk) of quartz sand. Single-grain dating was exclusively used to date the Holocene arroyo fill allosequences (n=49 samples, 600-5600 grains analyzed per sample), while Pleistocene deposits were dated using small aliquot analysis (n=5 samples, 44-55 aliquots analyzed per sample). Equivalent dose (D_E) values were calculated using the minimum age model (MAM) for Holocene samples and the central age model (CAM) (Galbraith and Roberts, 2012) for Pleistocene samples, as well as Holocene samples lacking significant positive skew. Samples with evidence of partial bleaching as indicated by significant positive skew were calculated using the MAM.

Optical signals detected through 7.5 mm UV filters (U-340) on Risø TL/OSL Model DA-20 readers at 125°C with a green laser (532 nm, at 135 mW/cm^2) as the stimulation source for single-grain analysis and blue-green light emitting diodes (LED) (470 nm at 36-45 mW/cm^2) for small-aliquot measurements. For single-grain dating, the luminescence signals were measured over 1 s with a 0.1 s pause before and after stimulation, and the signal was calculated using the sum from 0.1-0.13 s of stimulation as peak and 0.67-0.92 s as background signal. Small aliquot stimulation was conducted over 40-45s, and the resultant signal was calculated by subtracting the average of the last 5 s (background signal) from the first 0.7 s of the signal decay curve. Preheat temperatures following administered and natural doses were 220-240°C for 10s and cutheat temperatures following test doses (5-10 Gy) were 160°C for 10s, as suggested from dose recovery results (see Fig. S26).

Dose-response curves were fit with linear or saturating-exponential fits to calculate equivalent dose (D_E) values. Grains/aliquots were rejected if they showed reduced signal in response to infrared stimulation (feldspar contamination, Duller, 2003), if the recycled dose was >30% of unity, if the signal measured at the zero dose step was >1 Gy, or if the natural D_E was higher than the largest regenerative dose given.

Dose-rate determination

Samples for environmental dose-rate determination were collected from a 30 cm diameter area surrounding the sample tube. Sediments were homogenized and representative samples were analyzed for radioisotope concentration using ICP-MS and ICP-AES techniques (Table S1). These concentration values were converted to dose rate following the conversion factors of Guérin et al. (2011) and beta attenuation values of Brennan et al. (2003) (see Table S1). Contribution of cosmic radiation to the dose rate was calculated using sample depth, elevation and latitude/longitude following Prescott and Hutton (1994). Total dose rates (Table S1) were calculated based on water content, radioisotope concentration, and cosmic contribution (Adamiec and Aitken, 1998; Aitken, 1998).

Equivalent Dose distributions:

Equivalent dose (D_E) distributions are shown in Figures S20 – S25 below. Overall, most of the Holocene arroyo-fill alluvial deposits showed signs of partial bleaching such as positive skew and high overdispersion in the D_E values. The MAM of Galbraith and Roberts (2012) was

applied to single-grain D_E distributions with significant positive skew or overdispersion values >25% in order to isolate the population of grains that were most likely bleached (optically reset) prior to deposition. Pleistocene-aged samples were dating using small aliquots and their D_E values were calculated using the CAM of Galbraith and Roberts (2012).

Error propagation:

Equivalent dose (D_E) values and OSL ages are reported at 2-sigma standard error and include errors related to instrument calibration, dose rate and equivalent dose calculations. Errors were calculated in quadrature using the methods of Aitken and Alldred (1972) and Guérin et al. (2011). To allow direct comparison between calibrated radiocarbon and OSL data, both types of data have been set to have a uniform datum of 2010 CE.

Assembling the Chronostratigraphic Records

Identification of episodes of arroyo entrenchment and aggradation was primarily based on identification of buttress unconformities and other stratigraphic evidence exposed at each study site and secondarily based on age control derived from radiocarbon and OSL dating. Buttress unconformities observed in the arroyo wall stratigraphy indicate episodes of paleoarroyo entrenchment followed by aggradation, and the presence of colluvial wedges suggest the passage of a significant period of time prior to burial. Buried paleosols indicate hiatuses in sediment deposition that may be associated with arroyo entrenchment. Therefore, the stratigraphic evidence provides a reliable indicator of the relative timing of each event. Sites exposing the greatest number of unconformities were used to guide the number of cut-fill events. Radiocarbon and OSL dating were then used to place the relative stratigraphic ages into a chronostratigraphic record with absolute ages.

Both radiocarbon and OSL dating are prone to issues that may overestimate the ages of deposits. Radiocarbon analyses on charcoal collected from fluvial systems may provide age overestimates because the radiocarbon age of the sample only dates the time of death of the wood, which may occur long before transport and deposition in alluvial packages in semi-arid environments (e.g. Schiffer, 1986; Baker, 1987; Huff, 2013). Further, there is high potential for reworking and re-deposition of charcoal from older deposits in these arroyo systems (e.g. Summa-Nelson and Rittenour, 2012; Huff, 2013). As such, radiocarbon dating only provides a maximum age of deposition. OSL dating of dryland fluvial sediments can also be challenging due to partial bleaching of the luminescence signal during transport, which can lead to age overestimates (Rittenour, 2008). Indeed, previous studies conducted within Kanab Creek (Summa-Nelson and Rittenour, 2012; Nelson and Rittenour, 2014) and in other regional drainages (Harvey et al., 2011; Hayden, 2011; Huff, 2013) have identified partial bleaching as a significant problem. While pairing single-grain SAR protocol analyses (Duller, 2008) with the minimum age model (MAM) of Galbraith and Roberts (2012) helps identify the population of grains likely reset during the most recent transport event, the potential for overestimating ages of deposits still exists. Accordingly, OSL and radiocarbon ages that are inconsistent with the stratigraphic evidence exposed at each site are considered to be overestimating the true ages of the deposits, and were not used to assemble the chronostratigraphic records.

SUPPLEMENTAL RESULTS

Sedimentology and Stratigraphy of Kanab Creek Paleoarroyo Fills

The lower Kanab Creek valley fill alluvium is predominately composed of very fine- to coarse-grained sands deposited in laterally-extensive, broadly tabular beds separated into unconformity and soil bound allostratigraphic units representing past periods of aggradation. Sediment colors in this reach are predominately hues of 10YR (yellowish-brown), 5YR (reddish-

brown), and 2.5 YR (red). These distinct colors of individual beds are the result of varying bedrock sources within the catchment. The yellowish-brown beds are composed of fine- to coarse-grained, moderately well- to well-sorted, sub- to well-rounded, quartz sand likely derived from the Jurassic eolian Navajo Formation exposed in the White Cliffs, upstream of the lower basin study area. The reddish-brown to red beds are composed of very fine- to coarse-grained, poorly- to moderately well-sorted, sub-angular to sub-rounded quartz sand with variable amounts of clay and silt, and are likely derived from the Jurassic to Triassic Kayenta and Moenave Formations of the Vermilion Cliffs.

The alluvial stratigraphy of the upper arroyo fill units are similar to those in the lower basin. They are characterized by very fine- to medium-grained sand, silt and clay, deposited predominately in broadly tabular beds. The generally finer-grained alluvial fills of the upper basin are due to the higher proportion of mudstone, shale, and limestone in the local bedrock of the upper basin. Sediment colors are predominately hues of 10YR (yellowish-brown), with occasional beds of 7.5YR (brown) and 5YR (reddish-brown). Values of the 10YR hues tend to be lower (more brown and gray) than the 10YR hues of the lower basin paleoarroyo fills. Sediments with hues of 5YR are moderately- to well-sorted, sub-rounded to rounded, quartz sand with variable amounts of silt and clay, and are predominately derived from the Eocene to Oligocene Claron Formation exposed in the Pink Cliffs. The relationship between sediment with hues of 7.5YR and 10YR and bedrock source is not clear, but they may originate from the Cretaceous Dakota Sandstone or the earthy member of the Mt. Carmel Formation.

Eleven sedimentary facies defined by their sedimentary structures and grain size were identified in the Kanab Creek paleoarroyo fills. Facies codes follow Miall (2000). Sandy facies reflecting channel-margin deposition include massive sand (Sm), horizontally laminated sand (Sh), and trough, low-angle, and ripple cross-laminated sands (St Sl, and Sr respectively). These facies are the most common and volumetrically abundant in the arroyo wall stratigraphy, and beds are broadly tabular and laterally extensive. Fine-grained facies deposited in low-energy marshes or cienega environments include thin, very fine-grained laminated sands, silts, and clay beds, often with variegated coloring (Fsm and Fsmv). These beds are often traceable for tens of meters, forming prominent marker beds in the arroyo-wall stratigraphy. Relatively coarse facies deposited in axial channel thalweg include medium- to coarse-grained sand and matrix- or clast-supported gravels in lenticular beds that are typically massive (Gm) or imbricated / crossbedded (Gt). Thick (up to ~6 meters) and laterally extensive (broadly lenticular or tabular over tens of meters) gravel deposits are common in the lower half of arroyo wall exposures in the lower basin. These deposits return Pleistocene OSL ages (Table 1) and are interpreted to result from alluvial fan progradation from the base of the Vermilion Cliffs under a significantly different, pre-arroyo geomorphic, climatic and hydrologic regime.

Colluvial wedge deposits (VSc) typically mantle buttress unconformities in the arroyo-wall stratigraphy. Colluvial wedges are poorly-sorted and commonly contain rip-up clasts and blocks of cohesive older sediment derived from older arroyo wall alluvium. These deposits are similar to colluvial wedge mass failure and slope-mantling deposits at the base of modern arroyo wall exposures, and were deposited at the base of paleoarroyo walls following entrenchment. The presence of VSc deposits covering buttress unconformities likely indicates channel entrenchment for a significant period of time, which helps distinguish vertical buttress unconformities produced by >5 m arroyo channel entrenchment than minor unconformities produced by lateral channel migration. Paleosols (P), which indicate former valley surfaces and periods of floodplain stability, are common in the arroyo-wall stratigraphy.

References Cited in Data Repository

Adamiec, G., Aitken, M.J. (1998). Dose-rate conversion factors: update. Ancient TL 16, 37- 50.

Aitken, M.J. and Alldred, J.C., 1972. The assessment of error limits in thermoluminescent dating. Archaeometry 14, 257-267.

Aitken, M.J., 1998. An Introduction to Optical Dating. Oxford University Press, Oxford.

Brennan, B.J., 2003. Beta doses to spherical grains. Radiation Measurements 37, 299-303.

Duller, G.A.T., 2003. Distinguishing quartz and feldspar in single grain luminescence measurements. Radiation Measurements 37, 161-165.

Baker, V., 1987, Paleoflood hydrology and extraordinary flood events: Journal of Hydrology v. 96, p. 79-99.

Galbraith, R.F., and Roberts, R.G., 2012, Statistical aspects of equivalent dose and error calculation and display in OSL dating: An overview and some recommendations: Quaternary Geochronology, v. 11, p. 1-27.

Guerin, G., Mercier, N., and Adamiec, G., 2011, Dose-rate conversion factors: update: Ancient TL, v. 29, p. 5-8.

Harvey, J.E., Pederson, J.L., and Rittenour, T.M., 2011, Exploring relations between arroyo cycles and canyon paleoflood records in Buckskin Wash, Utah; Reconciling scientific paradigms: GSA Bulletin, v. 123, p. 2266-2276.

Hayden, A.E., 2011, Reconstructing the Holocene Arroyo History of the Upper Escalante River, Southern Utah, Using Optically Stimulated Luminescence (OSL) and Radiocarbon Dating: Masters Thesis, Utah State University, Logan, UT.

Hayden, J.M., 2011: Geologic map of the Kanab 7.5' Quadrangle, Kane County, Utah and Coconino and Mohave Counties, Arizona., Scale 1:24,000: Utah Geological Survey Map 248DM Plates 1-2.

Howard, A.D., and Kerby, G., 1983, Channel changes in badlands: Geological Society of America Bulletin, v. 94, p. 739-752.

Huff, W.M., 2013, A middle to late Holocene record of arroyo cut-fill events in Kitchen Corral Wash, southern Utah: Unpublished Masters Thesis, Utah State University, Logan, UT.

Huntley, D.J., Godfrey-Smith, D.I., and Thewalt, M.L.W., 1985, Optical dating of sediments: Nature, v. 313, p. 105-107.

Miall, AD, 2000, Principles of sedimentary basin analysis, 3rd ed. Springer, New York.

Murray, A.S., Wintle, A.G., 2000, Luminescence dating of quartz using an improved single-aliquot regenerative-dose protocol: Radiation Measurements v. 32, p. 57-73.

Nelson, M.S., and Rittenour, T.M., 2014, Middle to Late Holocene chronostratigraphy of alluvial fill deposits along Kanab Creek in southern Utah: Utah Geological Association Publication 43, 18 p.

Prescott, J.R., Hutton, J.T., 1994, Cosmic ray contributions to dose rates for luminescence and ESR dating: large depths and long-term time variations: Radiation Measurements v. 23, p. 497-500.

Rittenour, T.M., 2008, Luminescence dating of fluvial deposits: applications to geomorphic, paleoseismic and archaeological research. Bores, v. 37, p. 613-635.

Schiffer, M.B., 1986, Radiocarbon dating and the “old wood” problem: the case of the Hohokan chronology: Journal of Archaeological Sciences v. 13, p. 13-30.

Summa-Nelson, M.C., and Rittenour T.M., 2012, Application of OSL dating to middle to Late Holocene arroyo sediments in Kanab Creek, southern Utah, USA: Quaternary Geochronology, v. 10, p. 167-174.

Whipple, K.X., and Tucker, G.E., 1999, Dynamics of the stream-power river incision model: Implications for the height limitof mountain ranges, landscape responde time scale, and research needs: Journal of Geophysical Research, v. 104, n. 17, p. 661-674.

Table S1: Small-aliquot and Pleistocene OSL ages

USU Lab ID	Site ID	Depth (m)	Dep. Unit[1]	n[2]	Dose Rate[3] (Gy/ka)	Equivalent Dose[4] ± 2σ (Gy)	OSL Age ± 2σ (ka)
USU-263	21	5	Qf1	25 (53)	1.55 ± 0.06	9.02 ± 1.43	**5.83 ± 1.04**
USU-114	25	12.2	P	29 (55)	0.87 ± 0.04	12.09 ± 1.97	**13.86 ± 2.55**
USU-1754	24	7.9	P	19 (51)	0.51 ± 0.05	35.82 ± 3.14[5]	**70.83 ± 10.78**
USU-365	25	6.6	P	26 (50)	0.56 ± 0.03	42.00 ± 3.42[5]	**75.50 ± 9.38**
USU-1525	3	13	P	16 (846)	1.32 ± 0.05	101.96 ± 17.45[5]	**77.18 ± 14.61**
USU-1627	26	11.9	P	18 (44)	0.90 ± 0.04	82.29 ± 10.95[5]	**91.59 ± 15.18**

[1] Depositional Unit codes: P= Pleistocene, H= Holocene, Qf1 = Quaternary fill 1.

[2] Number of aliquots used in age calculation, and number of aliquots analyzed in parentheses.

[3] Dose rate, from radioelemental concentrations of U, Th, K, Rb measured using ICP-MS and ICP-AES techniques, is derived by conversion factors from Guérin et al. (2011) and cosmic radiation was calculated using sample depth, elevation, and latitude/longitude following Prescott and Hutton (1994). See Supplemental Table S2 for details.

[4] Equivalent dose (D_E) determined using the single-aliquot regenerative-dose procedure of Murray and Wintle (2000) on 1-mm small-aliquots of quartz sand, and Minimum Age Model of Galbraith and Roberts (2012) unless otherwise noted.

[5] Equivalent dose (D_E) determined using the Central Age Model of Galbraith and Roberts (2012).

Table S2: OSL dose rate information.

USU Lab ID[1]	In-situ H_2O[1] (%)	%K[2]	Rb[2] (ppm)	Th[2] (ppm)	U[2] (ppm)	Cosmic	Dose Rate (Gy/ka)
USU-114	0.2	0.60	22.0	1.5	0.5	0.07	0.87 ± 0.04
USU-115	1.1	1.30	45.9	2.9	1.1	0.03	1.75 ± 0.07
USU-263	0.8	1.05	42.2	2.6	0.8	0.15	1.55 ± 0.06
USU-285	0.5	0.38	17.0	0.9	0.4	0.17	0.70 ± 0.04
USU-286	0.4	0.78	27.6	1.1	0.4	0.20	1.13 ± 0.05
USU-287	0.4	0.55	24.5	1.2	0.5	0.25	0.99 ± 0.05
USU-290	0.1	0.79	22.8	0.9	0.4	0.20	1.13 ± 0.05
USU-292	0.5	0.64	21.9	0.9	0.4	0.17	0.95 ± 0.05
USU-356	1.7	0.99	30.9	1.4	0.5	0.14	1.33 ± 0.06
USU-359	0.2	0.74	27.6	1.3	0.4	0.22	1.12 ± 0.05
USU-360	0.4	0.65	24.0	1.0	0.3	0.14	0.91 ± 0.05
USU-361	0.4	1.24	45.8	1.8	0.6	0.25	1.73 ± 0.07
USU-362	1.5	0.46	18.1	1.7	0.6	0.24	0.94 ± 0.05
USU-363	1.4	0.54	20.1	1.0	0.4	0.02	0.71 ± 0.04
USU-364	0.4	0.70	26.4	1.3	0.4	0.20	1.05 ± 0.05
USU-365	0.1	0.31	11.6	0.9	0.4	0.12	0.56 ± 0.03 [3]
USU-423	0.4	1.30	44.8	1.8	0.6	0.04	1.58 ± 0.06
USU-424	2.8	0.84	30.3	1.3	0.5	0.02	1.05 ± 0.05
USU-445	0.2	0.73	27.0	1.3	0.5	0.16	1.08 ± 0.05
USU-446	0.9	0.75	33.1	3.4	0.9	0.06	1.23 ± 0.05
USU-519	8.2	1.76	68.8	3.8	1.2	0.11	2.38 ± 0.09
USU-520	0.3	0.72	26.2	1.2	0.4	0.24	1.12 ± 0.05
USU-1030	1.2	0.80	32.2	1.3	0.5	0.11	1.08 ± 0.05
USU-1031	1.5	0.80	33.1	0.8	0.3	0.17	1.06 ± 0.05
USU-1428	9.1	1.07	51.7	5.1	1.7	0.12	1.87 ± 0.10
USU-1474	-	1.35	67.4	7.3	1.9	0.18	2.40 ± 0.13
USU-1520	0.2	1.31	43.1	2.1	0.8	0.06	1.63 ± 0.09 [3]
USU-1522	0.2	0.85	28.7	1.1	0.5	0.09	1.09 ± 0.06
USU-1523	0.5	1.27	40.4	1.4	0.5	0.05	1.47 ± 0.08
USU-1524	0.4	1.09	34.2	1.0	0.4	0.11	1.30 ± 0.07
USU-1525	-	0.82	33.5	3.6	1.1	0.07	1.32 ± 0.05
USU-1531	3.2	0.49	15.7	1.9	0.7	0.25	1.01 ± 0.05
USU-1627	1.6	0.67	22.7	1.4	0.5	0.07	0.90 ± 0.04
USU-1628	2.8	1.72	57.4	2.8	1.0	0.07	2.13 ± 0.11
USU-1630	1.3	1.89	61.0	3.0	1.2	0.15	2.43 ± 0.13
USU-1737	0.1	0.34	11.7	0.7	0.3	0.05	0.48 ± 0.04 [3]
USU-1738	1.4	0.60	18.7	0.9	0.3	0.12	0.82 ± 0.05
USU-1739	1.3	1.13	33.6	1.3	0.4	0.03	1.28 ± 0.07
USU-1740	3.2	1.82	58.5	2.6	1.0	0.14	2.27 ± 0.12
USU-1741	0.1	1.75	61.1	2.2	0.7	0.05	2.06 ± 0.11
USU-1745	2.9	1.37	42.2	1.5	0.5	0.11	1.62 ± 0.06
USU-1746	1.3	0.98	35.2	1.2	0.4	0.10	1.21 ± 0.07
USU-1747	1.4	0.58	19.7	0.8	0.3	0.06	0.73 ± 0.05 [3]
USU-1748	0.6	1.31	40.3	1.2	0.5	0.15	1.59 ± 0.06
USU-1749	2.0	1.41	52.1	1.6	0.5	0.07	1.64 ± 0.09
USU-1750	0.3	1.44	43.9	1.2	0.5	0.11	1.67 ± 0.09
USU-1754	0.2	0.30	9.5	0.8	0.3	0.11	0.51 ± 0.05
USU-1755	0.4	1.86	67.7	4.1	1.6	0.16	2.56 ± 0.13 [3]
USU-1756	0.2	0.69	23.8	1.0	0.4	0.25	1.06 ± 0.06
USU-1758	0.0	0.43	13.6	0.8	0.4	0.17	0.72 ± 0.05
USU-1760	8.5	1.28	48.7	5.0	1.7	0.17	2.00 ± 0.11
USU-1761	3.2	1.12	43.6	3.2	1.0	0.20	1.71 ± 0.09
USU-1763	3.7	0.86	33.2	2.9	0.9	0.18	1.41 ± 0.08
USU-1870	0.6	0.46	15.3	0.8	0.3	0.09	0.66 ± 0.04

[1] Assumed 5% for Pleistocene samples and 3% for samples with in-situ values <3% and >5% as moisture content over burial history.

[2] Radioelemental concentrations determined by ICP-MS and ICP-AES techniques; dose rate is derived from concentrations by conversion factors from Guérin et al. (2011).

[3] Dose rate uses average of chemical concentrations from multiple subsamples

Table S3: Latitude and longitude of study sites.

Site ID	Latitude (degrees)	Longitude (degrees)
1	37.405	-112.473
2	37.301	-112.482
3	37.288	-112.496
4	37.285	-112.499
5	37.185	-112.537
6	37.176	-112.540
7	37.157	-112.518
8	37.144	-112.539
9	37.129	-112.542
10	37.124	-112.541
11	37.118	-112.545
12	37.110	-112.549
13	37.080	-112.538
14	37.074	-112.543
15	37.068	-112.538
16	37.068	-112.540
17	37.065	-112.542
18	37.061	-112.540
19	37.055	-112.539
20	37.049	-112.537
21	37.040	-112.534
22	37.040	-112.533
23	37.038	-112.533
24	37.031	-112.535
25	37.028	-112.536
26	37.018	-112.536
27	37.011	-112.536

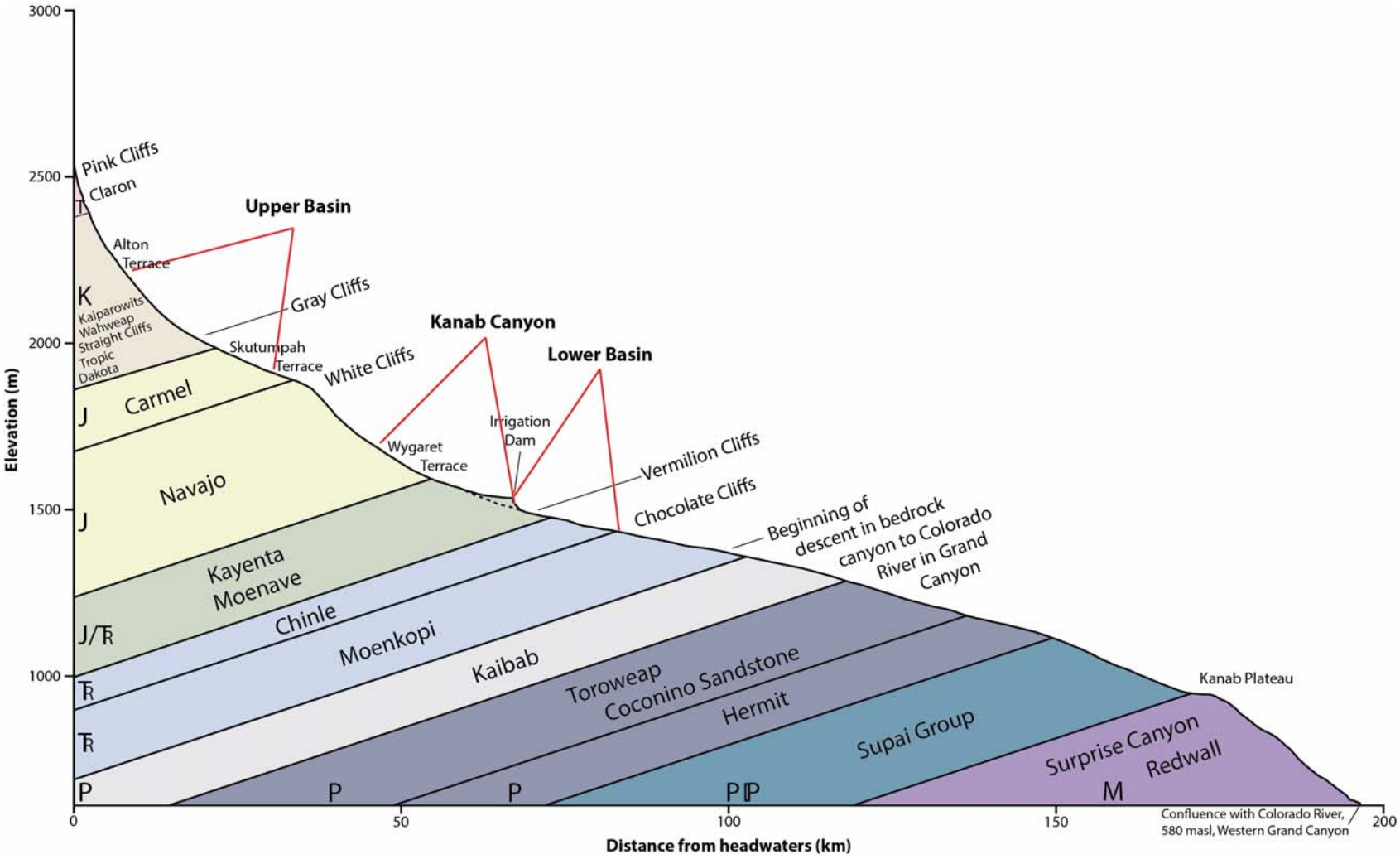

Fig. S1. Longitudinal profile and underlying bedrock of Kanab Creek from its headwaters to its confluence with Colorado River in Grand Canyon.

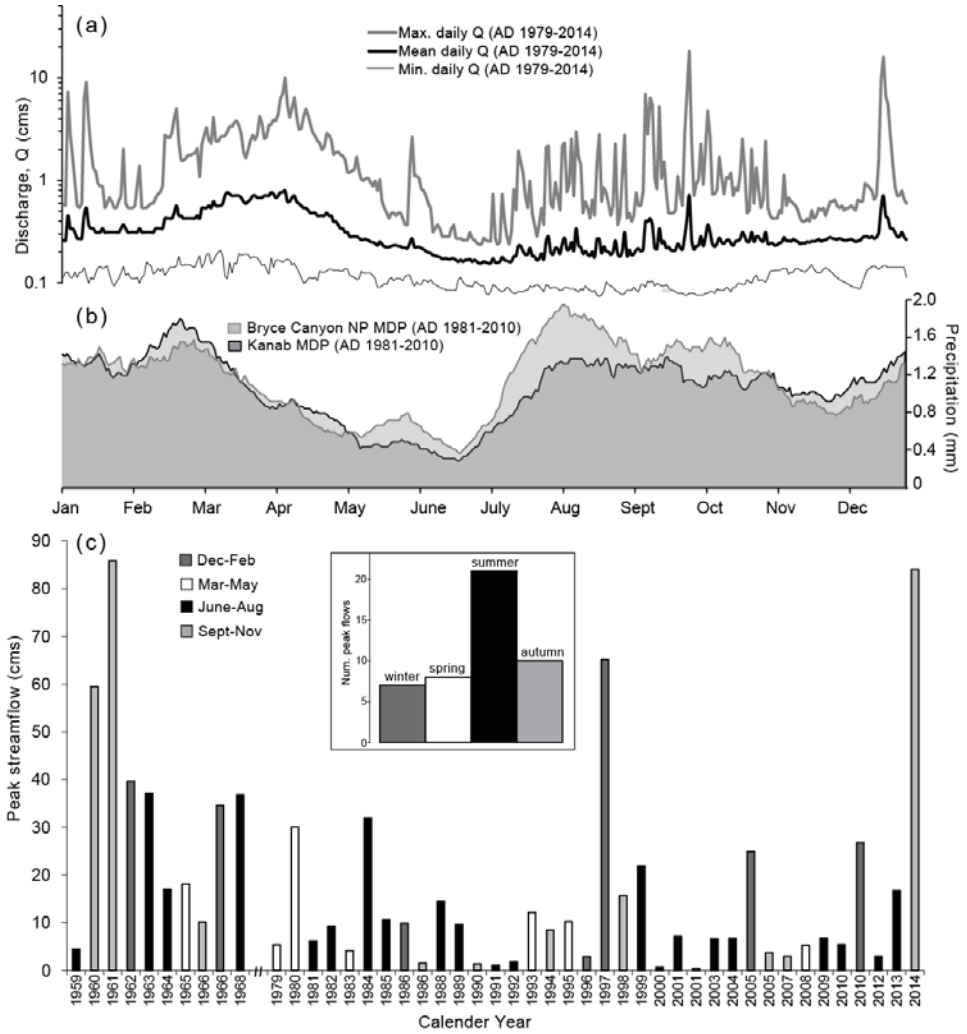

Fig. S2: Climate and hydrologic data near Kanab, UT. (a) Mean, maximum, and minimum daily discharge statistics, AD 1979-2014 for USGS Kanab Creek gage 9403600 (USGS, 2015). cms= cubic meters per second. (b) 30-year mean daily precipitation summary, AD 1981-2010 for Kanab station 424508 and Bryce Canyon National Park station 421008 (WRCC, 2015). (c) Peak annual streamflow 1959-2014, colors of bars relate to month of flood event. Inset histogram displays frequency of peak floods per month cluster/season.

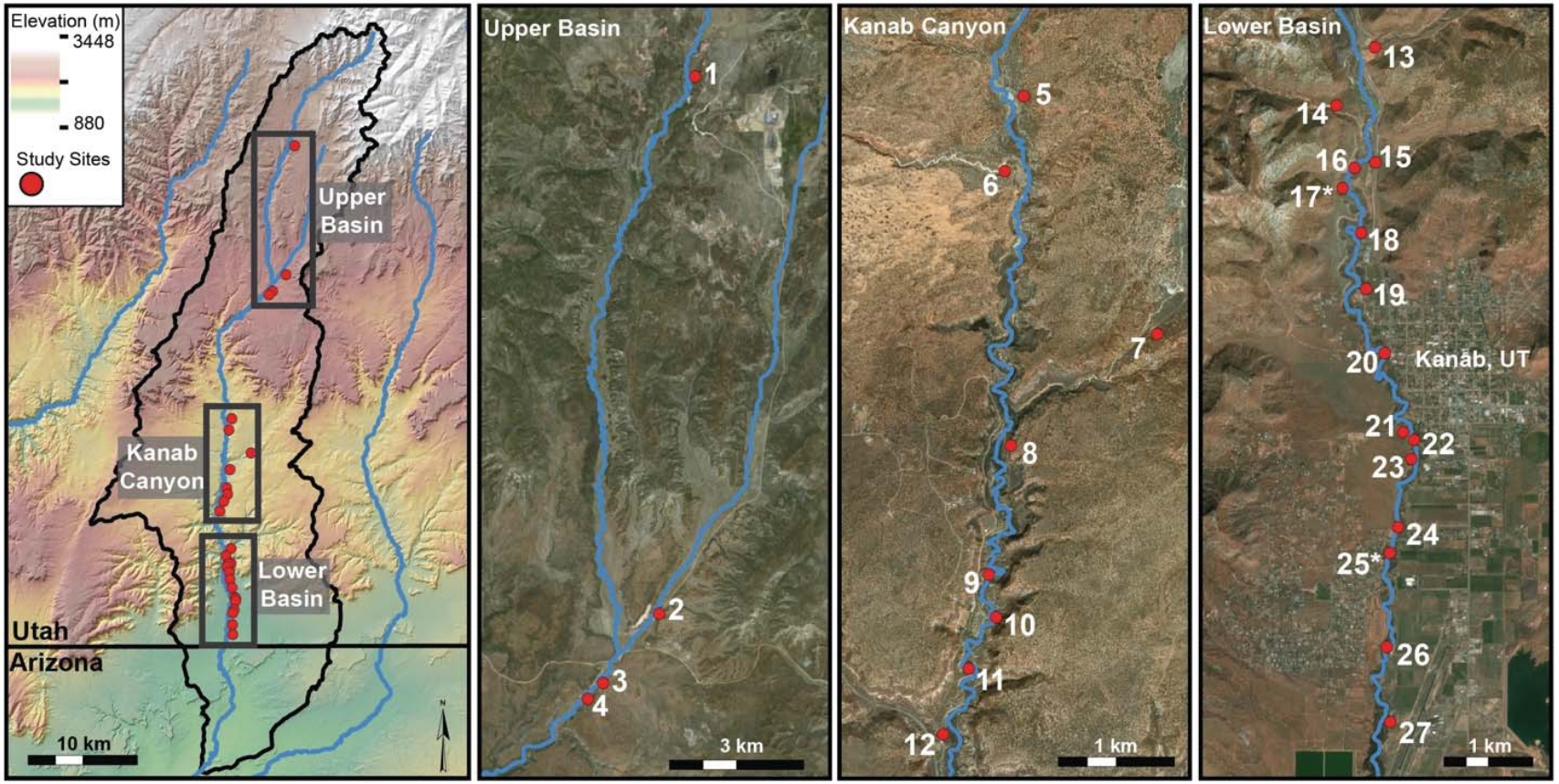

Fig. S3: Site locations along the upper basin, canyon, and lower basin reaches of Kanab Creek, southern Utah. Samples from sites 17 and 25 were collected by Hayden (2011). Stratigraphic panels are unavailable for these sites.

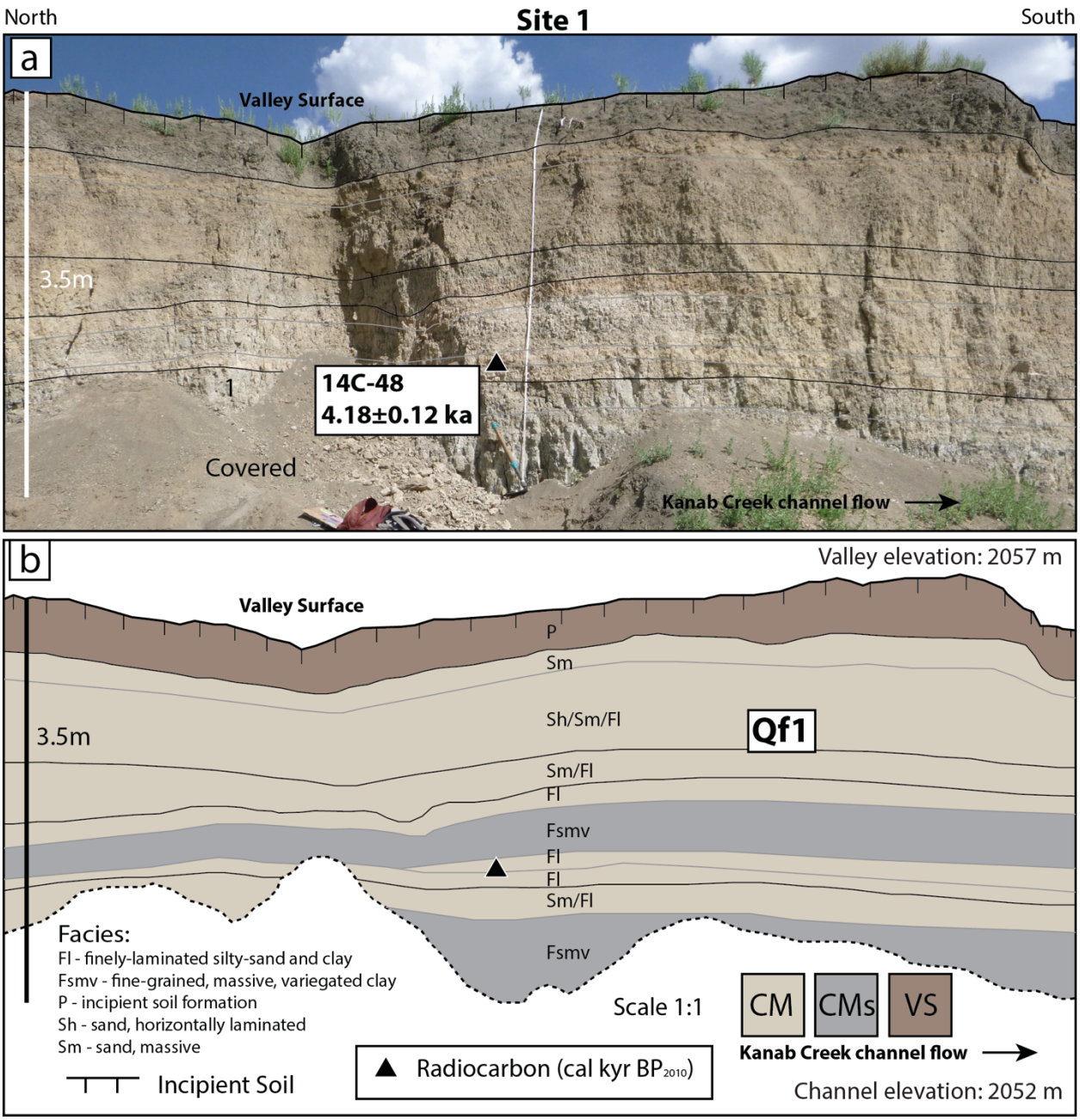

Fig. S4: Site 1 (a) annotated photo with location and age of geochronology samples, and (b) stratigraphic panel and interpreted alluvial fill number.

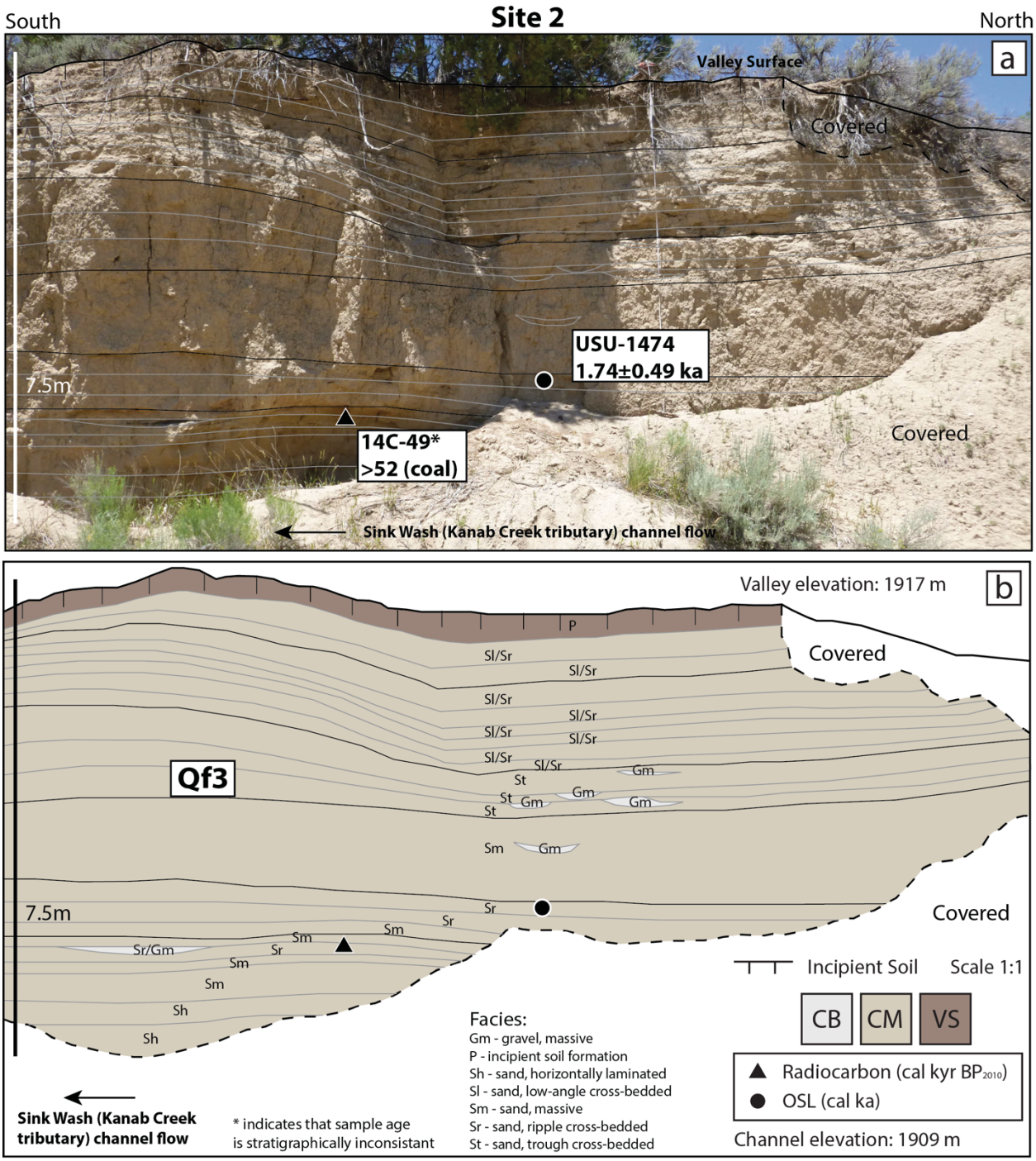

Fig. S5: Site 2 (a) annotated photo with location and age of geochronology samples, and (b) stratigraphic panel and interpreted alluvial fill number.

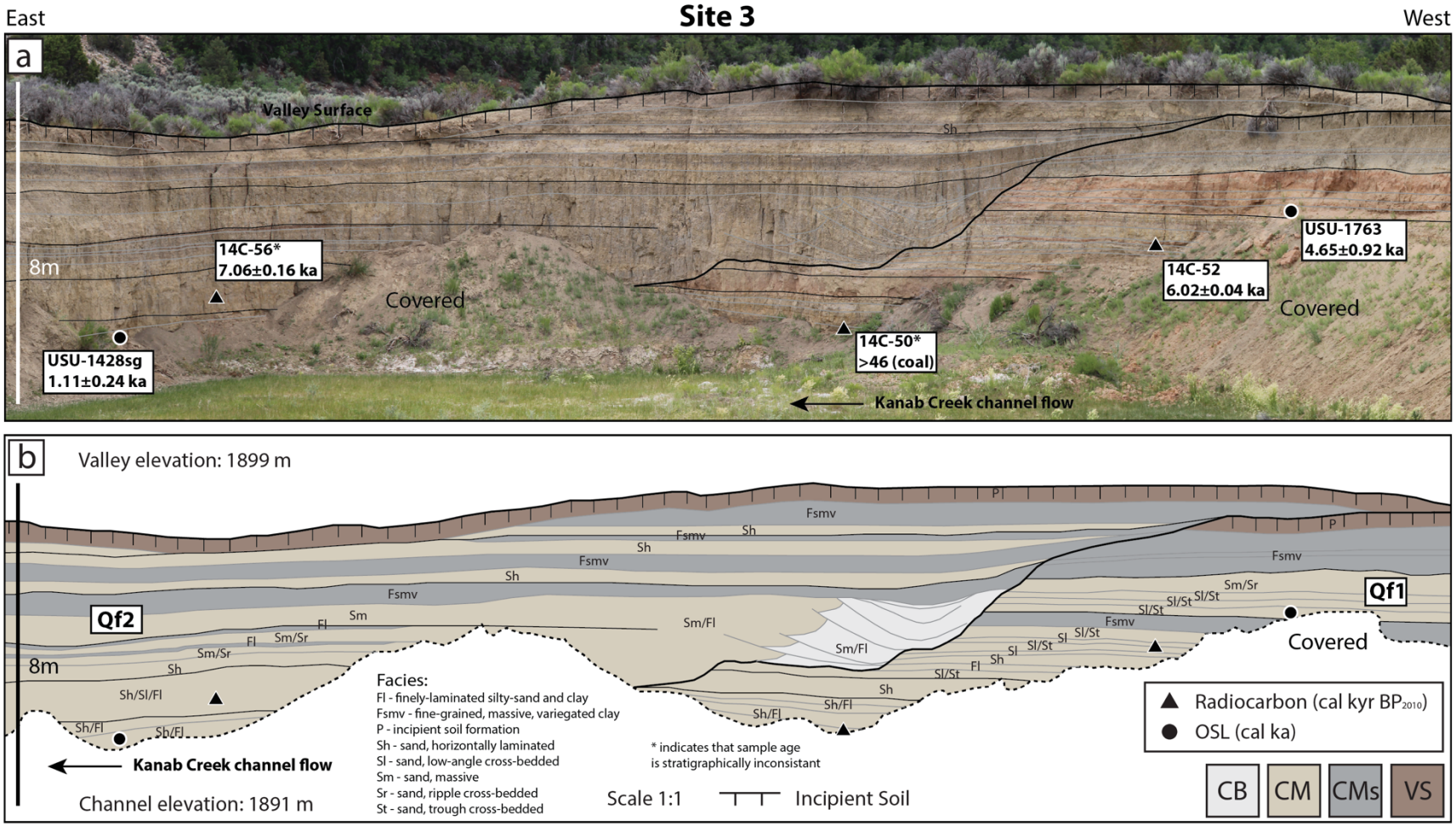

Fig. S6: Site 3 (a) annotated photo with location and age of geochronology samples, and (b) stratigraphic panel and interpreted alluvial fill number.

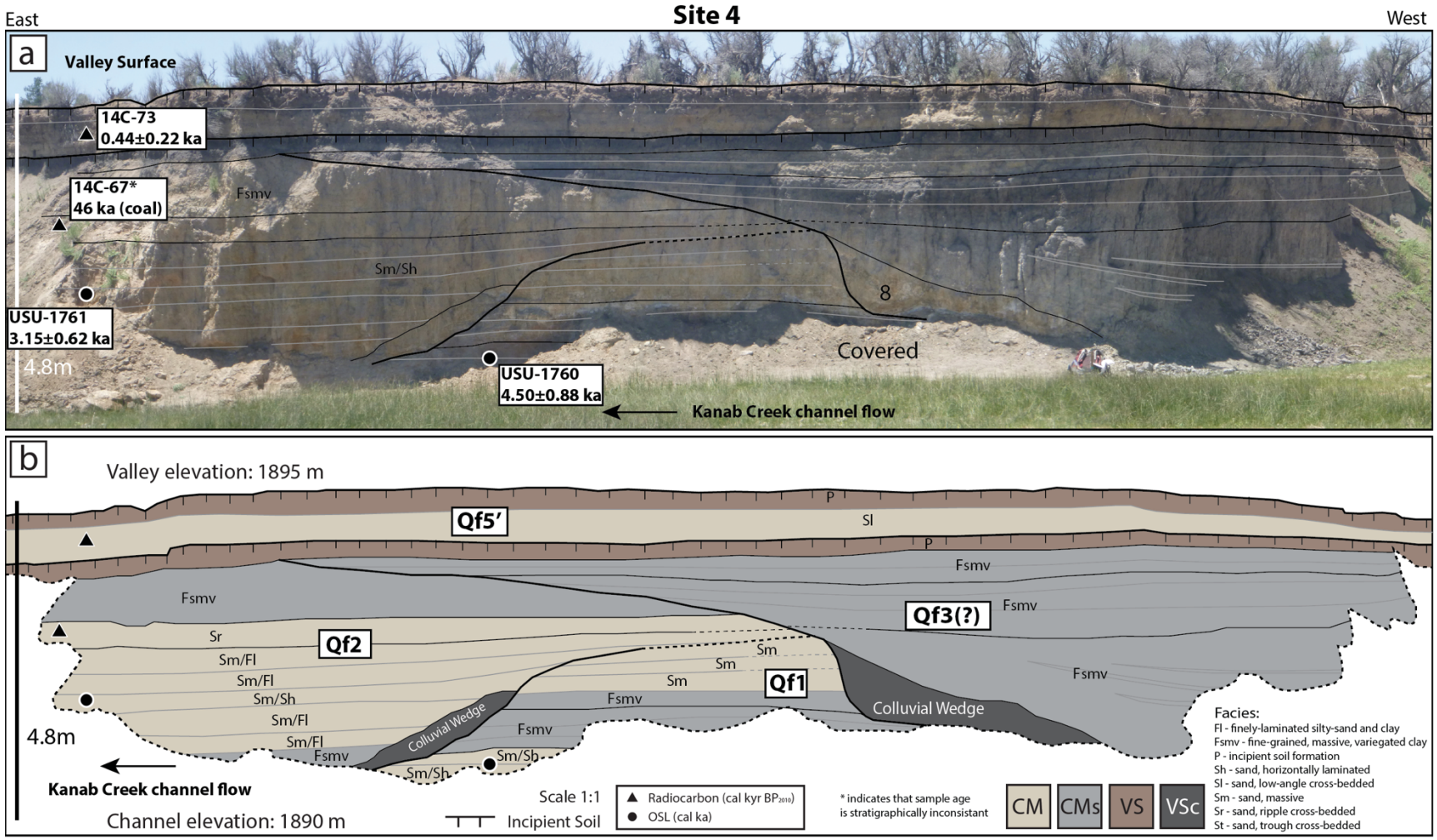

Fig. S7: Site 4 (a) annotated photo with location and age of geochronology samples, and (b) stratigraphic panel and interpreted alluvial fill number.

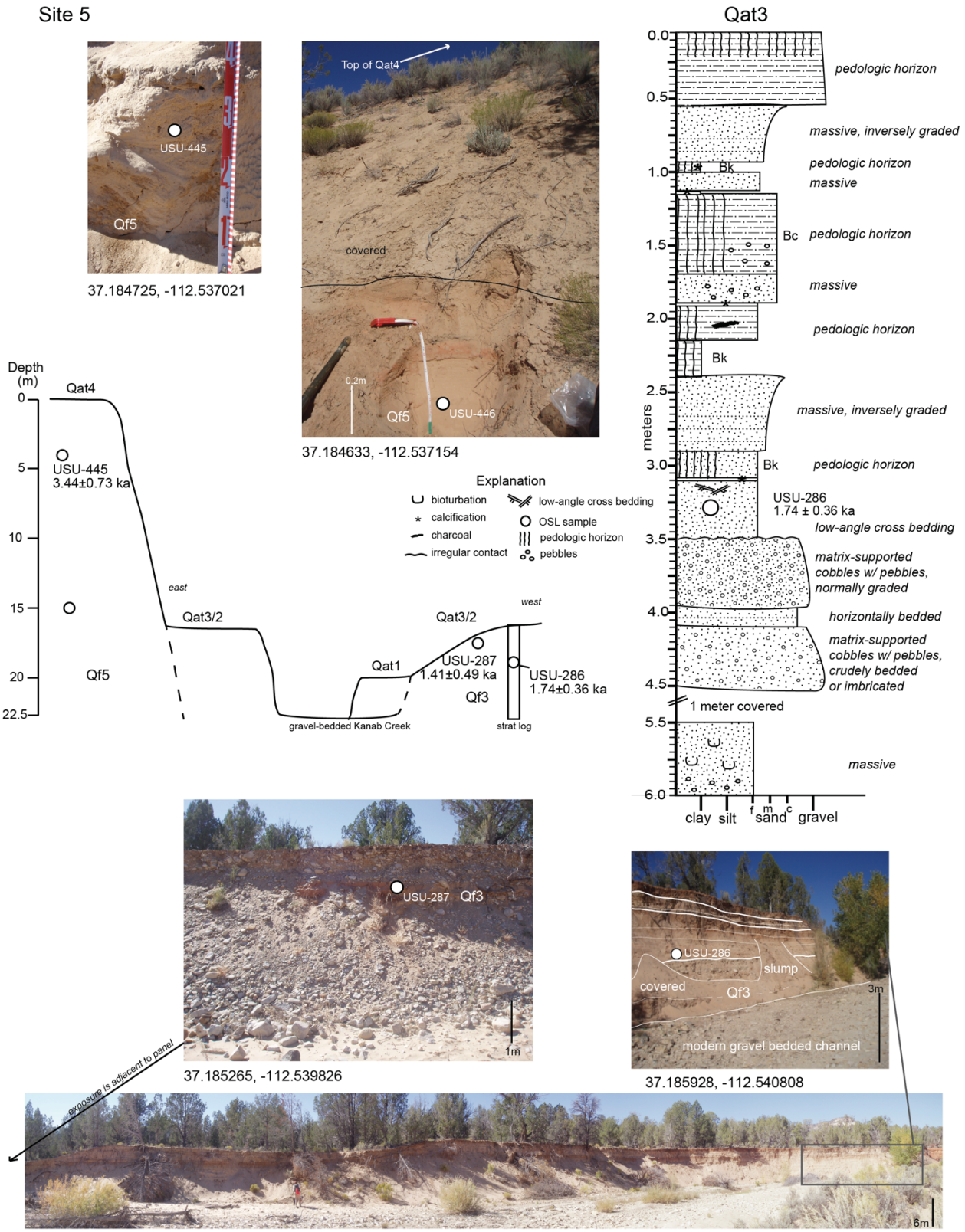

Fig. S8: Site 5 stratigraphic columns and annotated photos with location and age of geochronology samples. Site A from Nelson and Rittenour (2014).

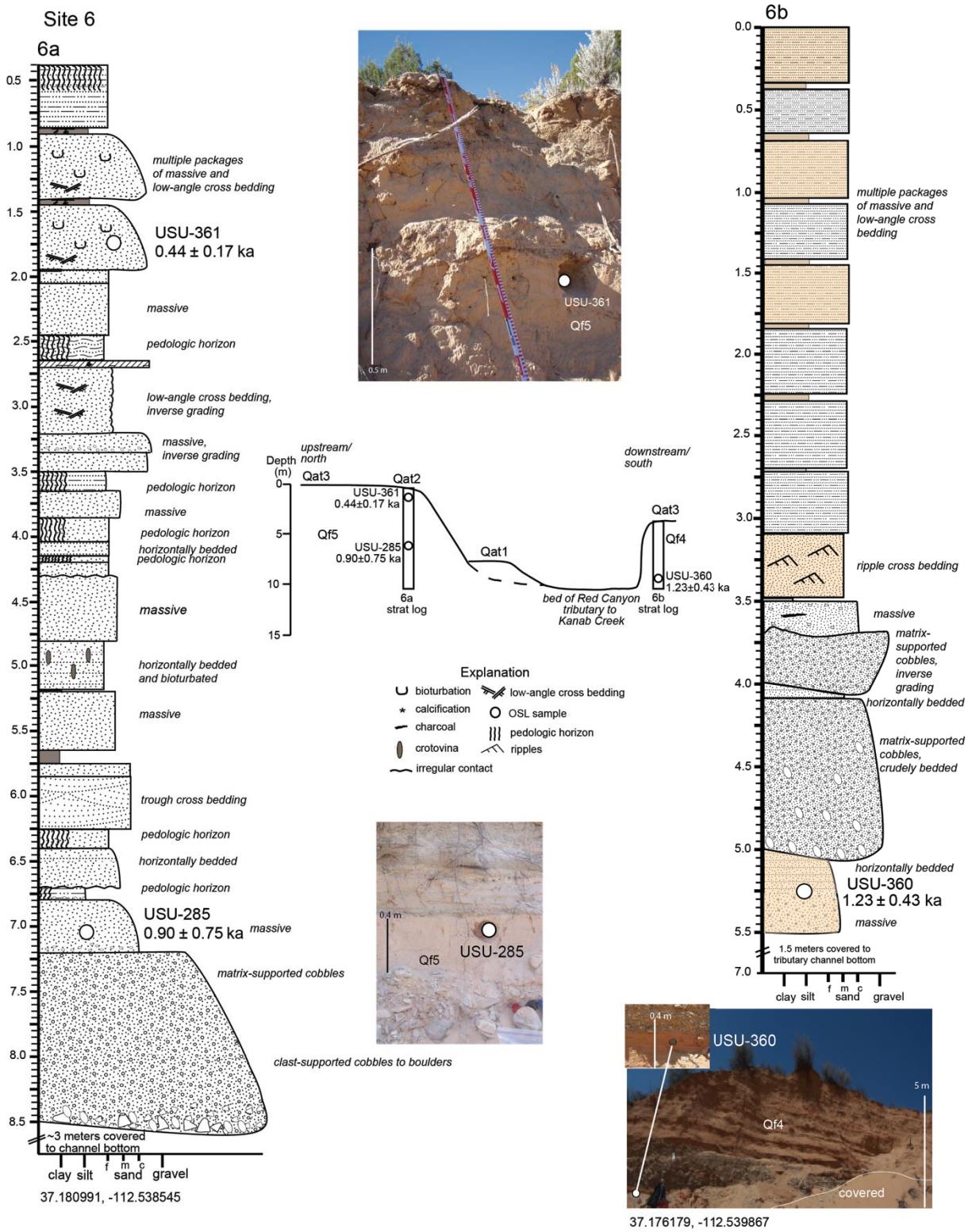

Fig. S9: Site 6 stratigraphic columns and annotated photos with location and age of geochronology samples. Site B from Nelson and Rittenour (2014).

Site 7 - John R. Canyon, tributary to Kanab Creek

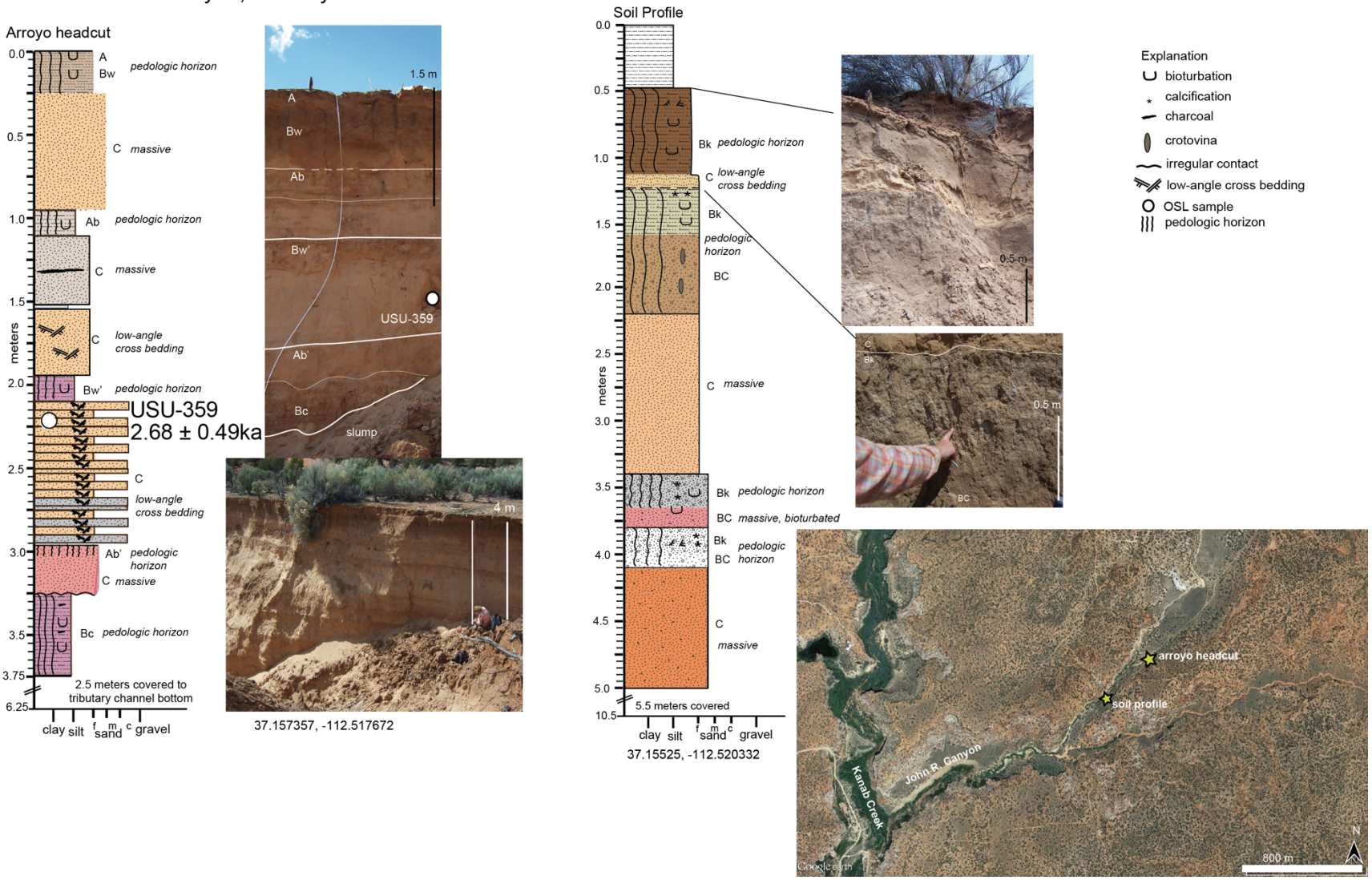

Fig. S10: Site 7 stratigraphic columns and annotated photos with location and age of geochronology samples. Site C from Nelson and Rittenour (2014).

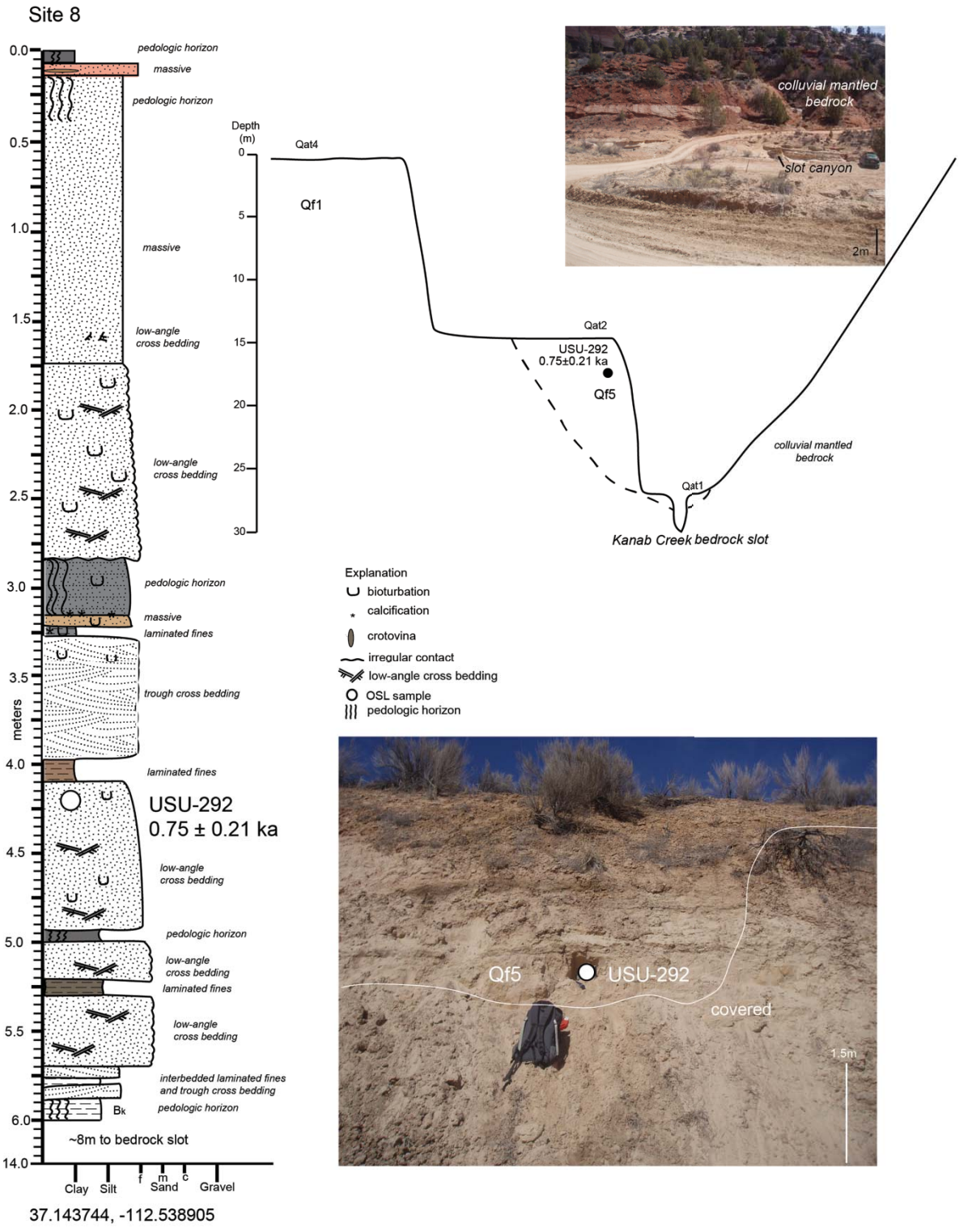

Fig. S11: Site 8 stratigraphic column and annotated photo with location and age of geochronology samples. Site D from Nelson and Rittenour (2014).

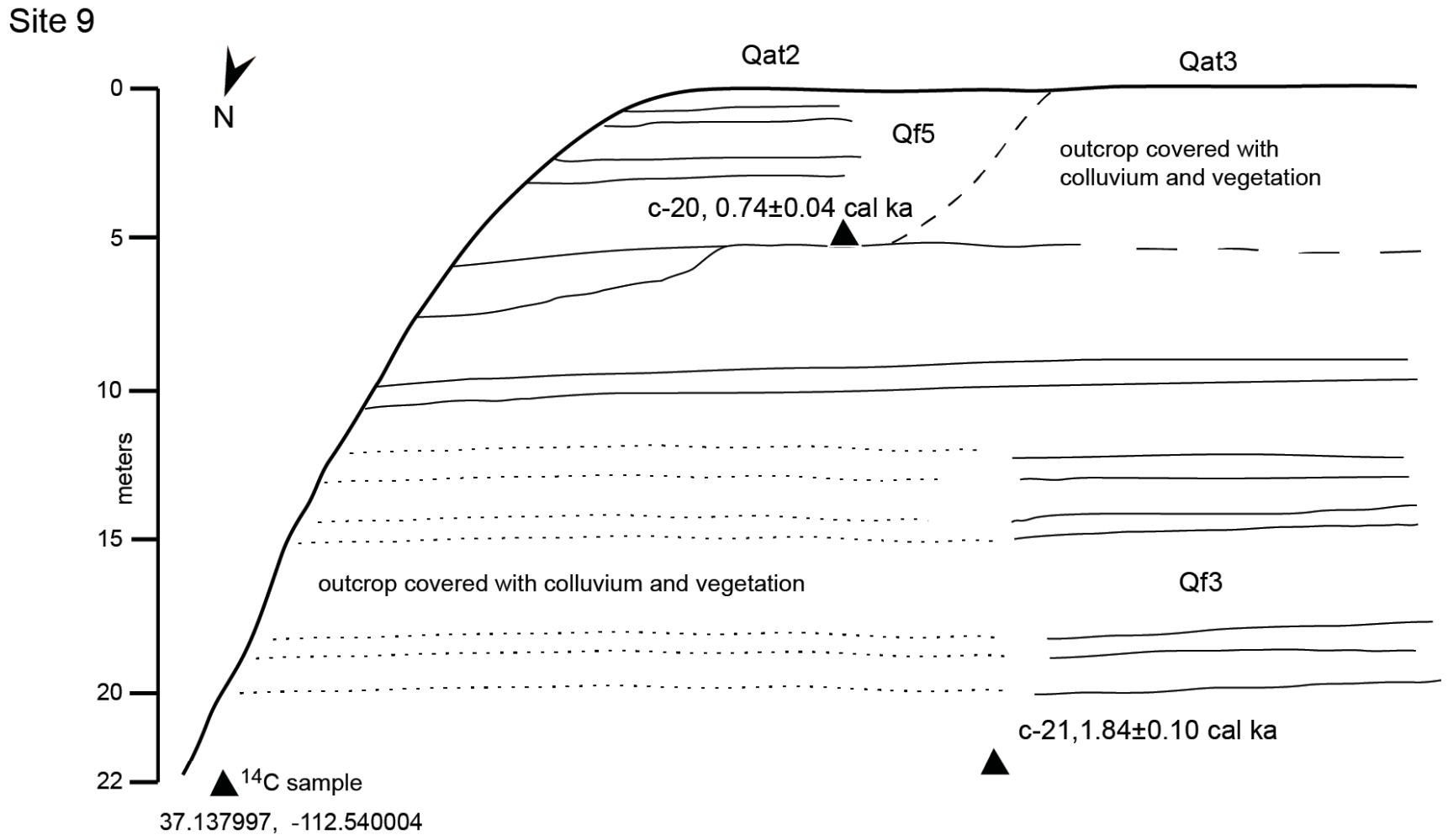

Fig. S12: Site 9 stratigraphic column with location and age of geochronology samples. Site E from Nelson and Rittenour (2014).

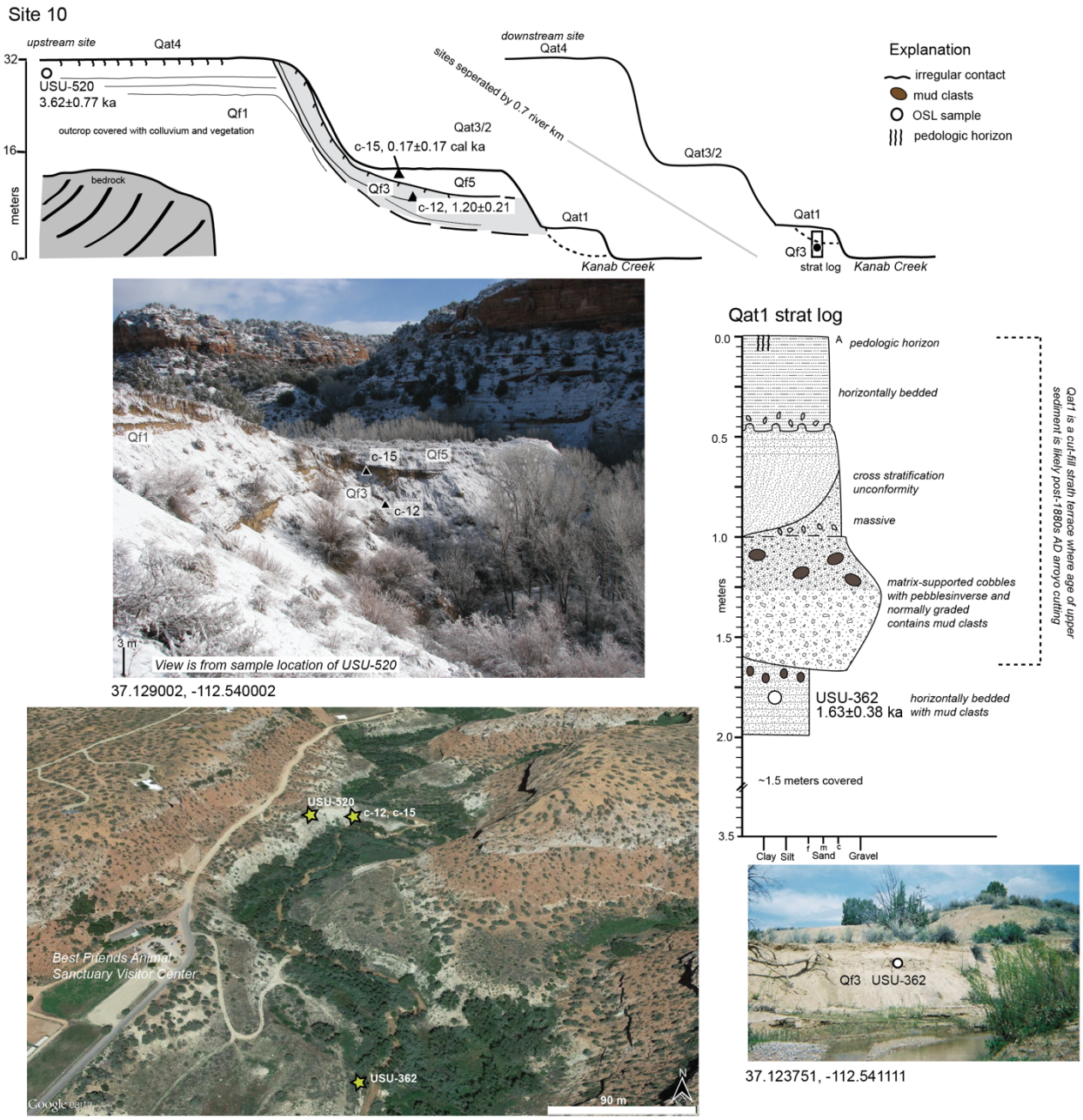

Fig. S13: Site 10 stratigraphic columns and annotated photos with location and age of geochronology samples. Site F from Nelson and Rittenour (2014).

Site 12

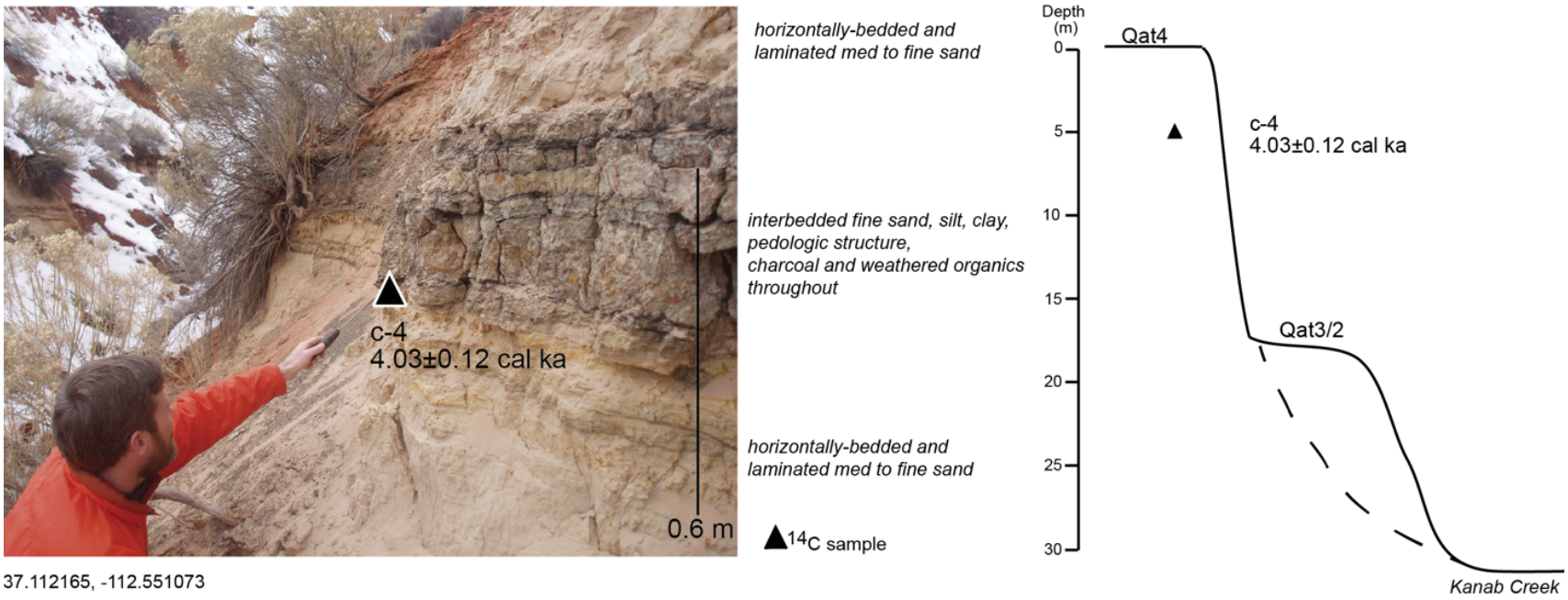

37.112165, -112.551073

Fig. S14: Site 12 stratigraphic descriptions and annotated photo with location and age of geochronology samples. Site H from Nelson and Rittenour (2014).

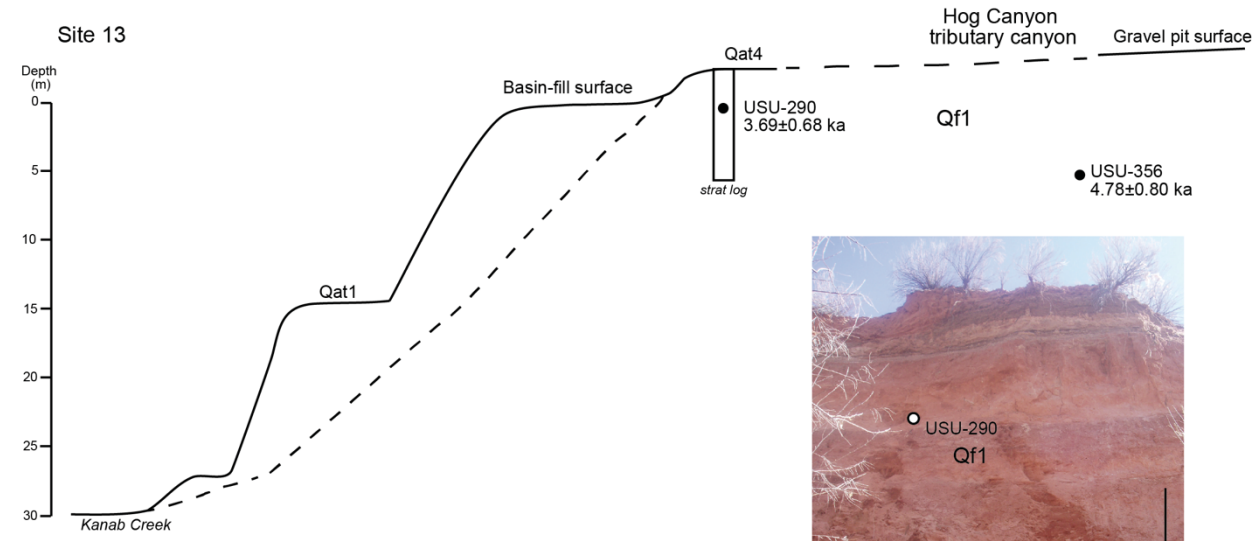

37.078489, -112.538766

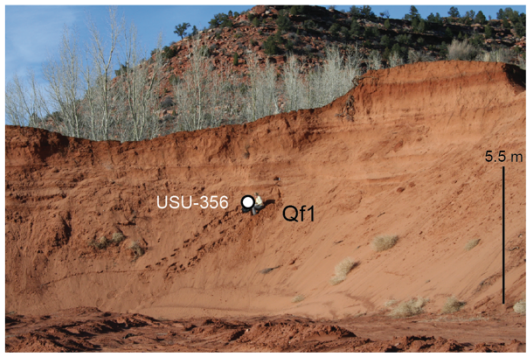

37.077903, -112.536684

OSL unit: 0.4-0.5 m thick light colored (wet 2.5YR6/8) lower fine to upper fine sand, low angle cross laminations, minor crotovina burrows.

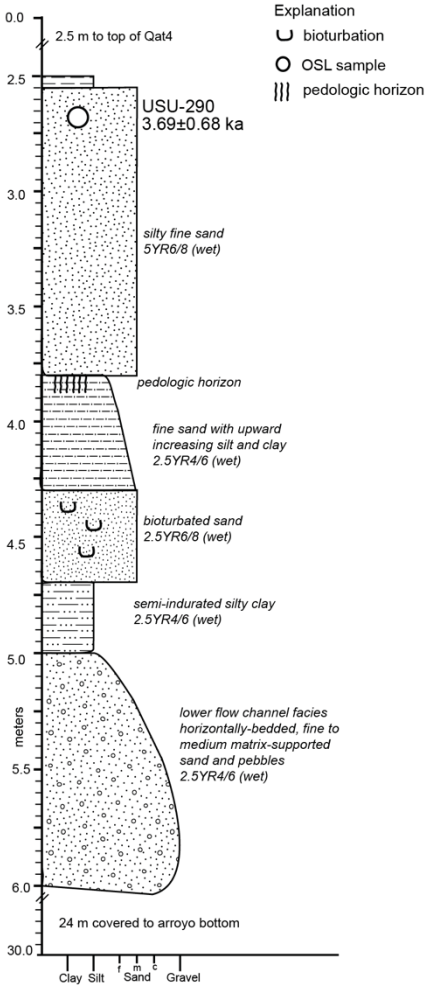

Fig. S15: Site 13 stratigraphic column and annotated photos with location and age of geochronology samples. Site I from Nelson and Rittenour (2014).

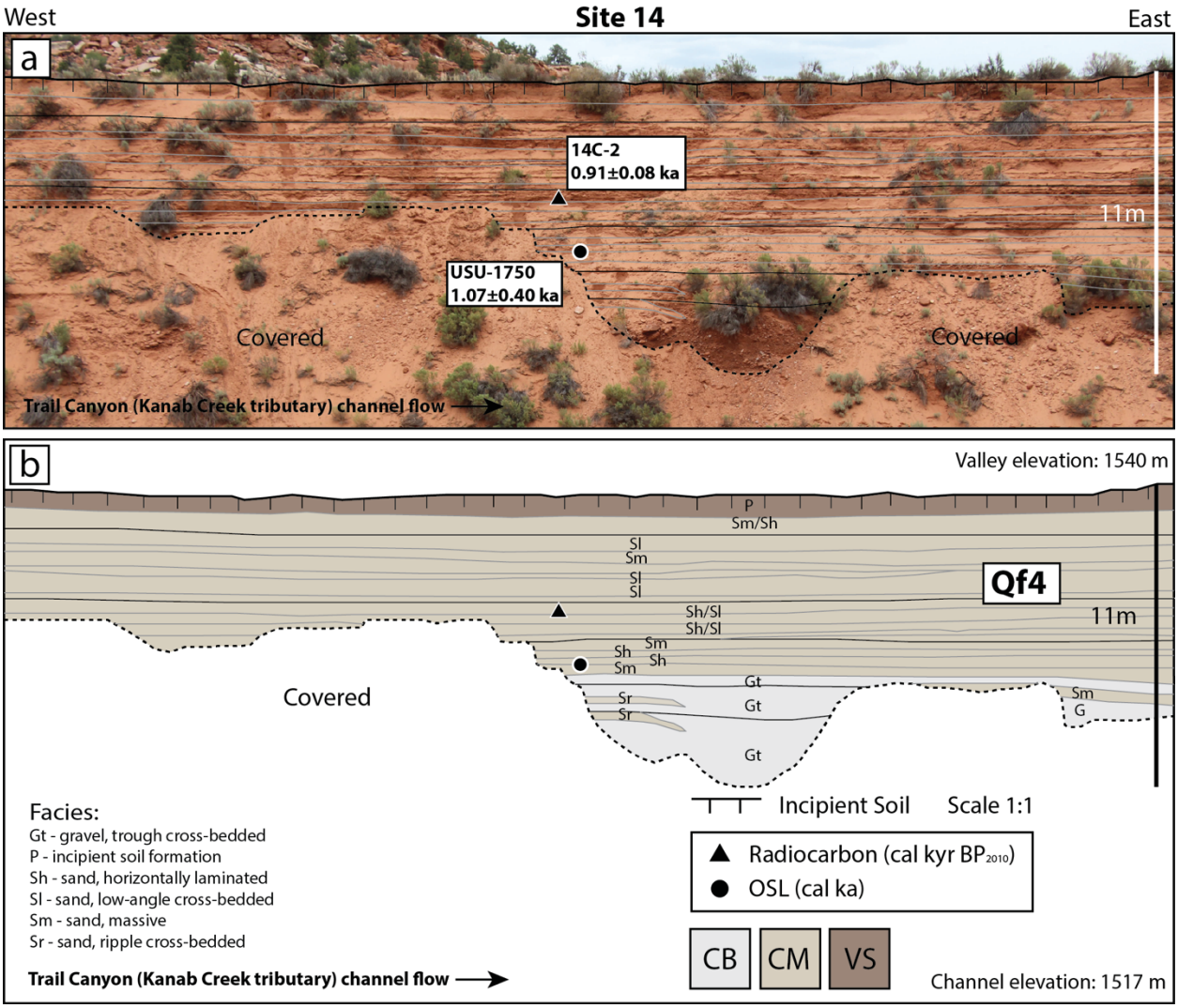

Fig. S16: Site 14 (a) annotated photo with location and age of geochronology samples, and (b) stratigraphic panel and interpreted alluvial fill number.

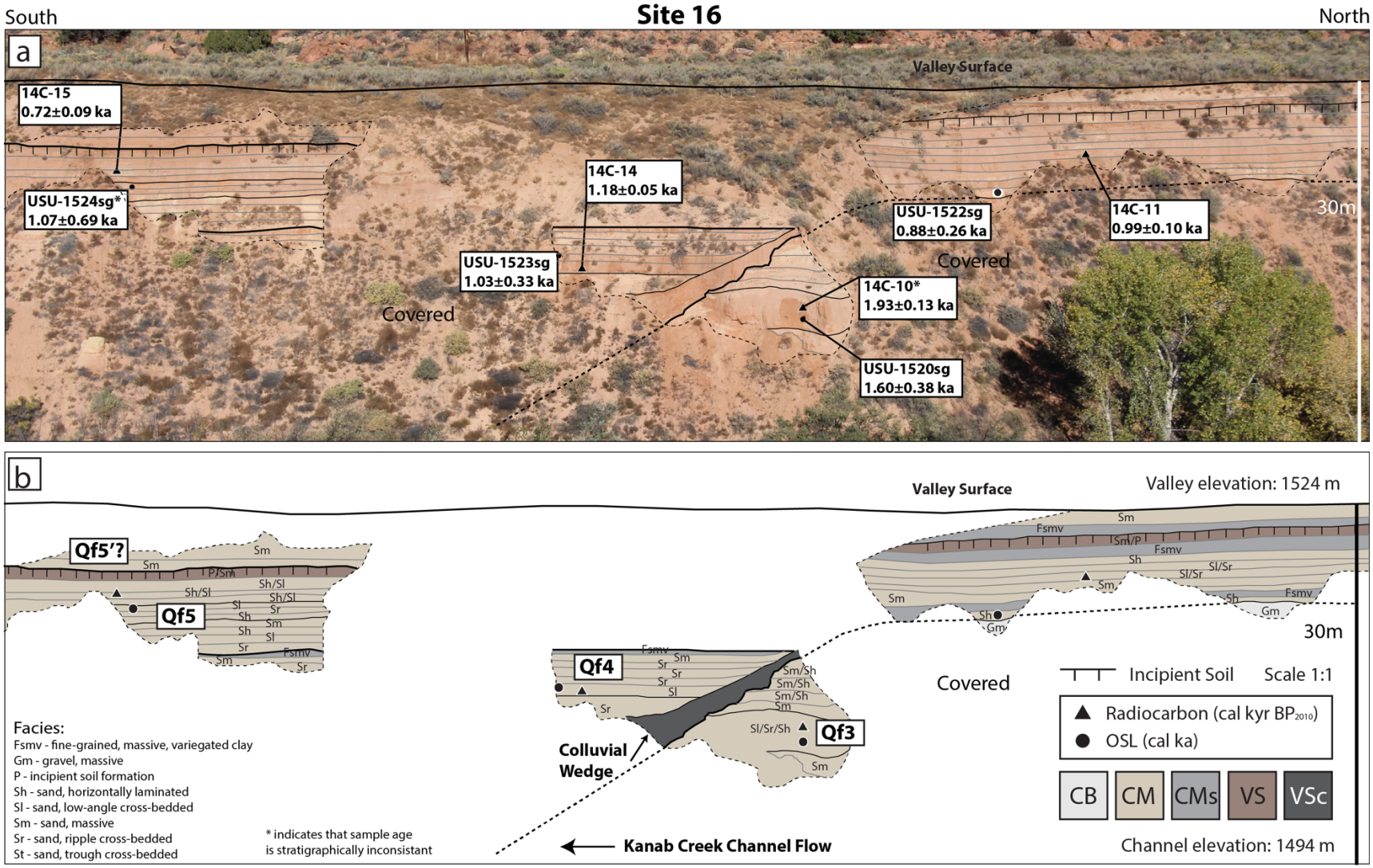

Fig. S17: Site 16 (a) annotated photo with location and age of geochronology samples, and (b) stratigraphic panel and interpreted alluvial fill number.

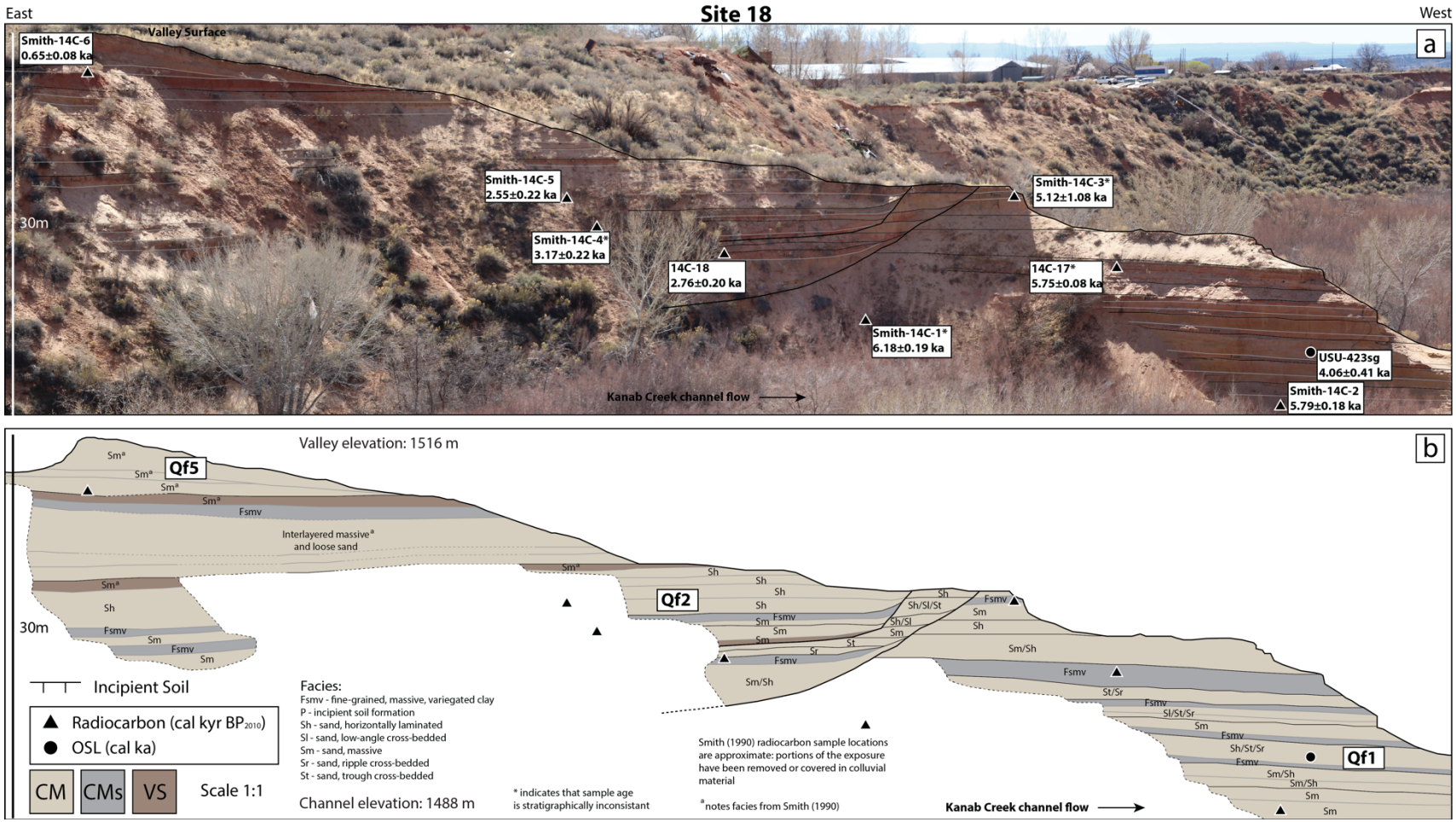

Fig. S18: Site 18 (a) annotated photo with location and age of geochronology samples, and (b) stratigraphic panel and interpreted alluvial fill number. Site K from Nelson and Rittenour (2014).

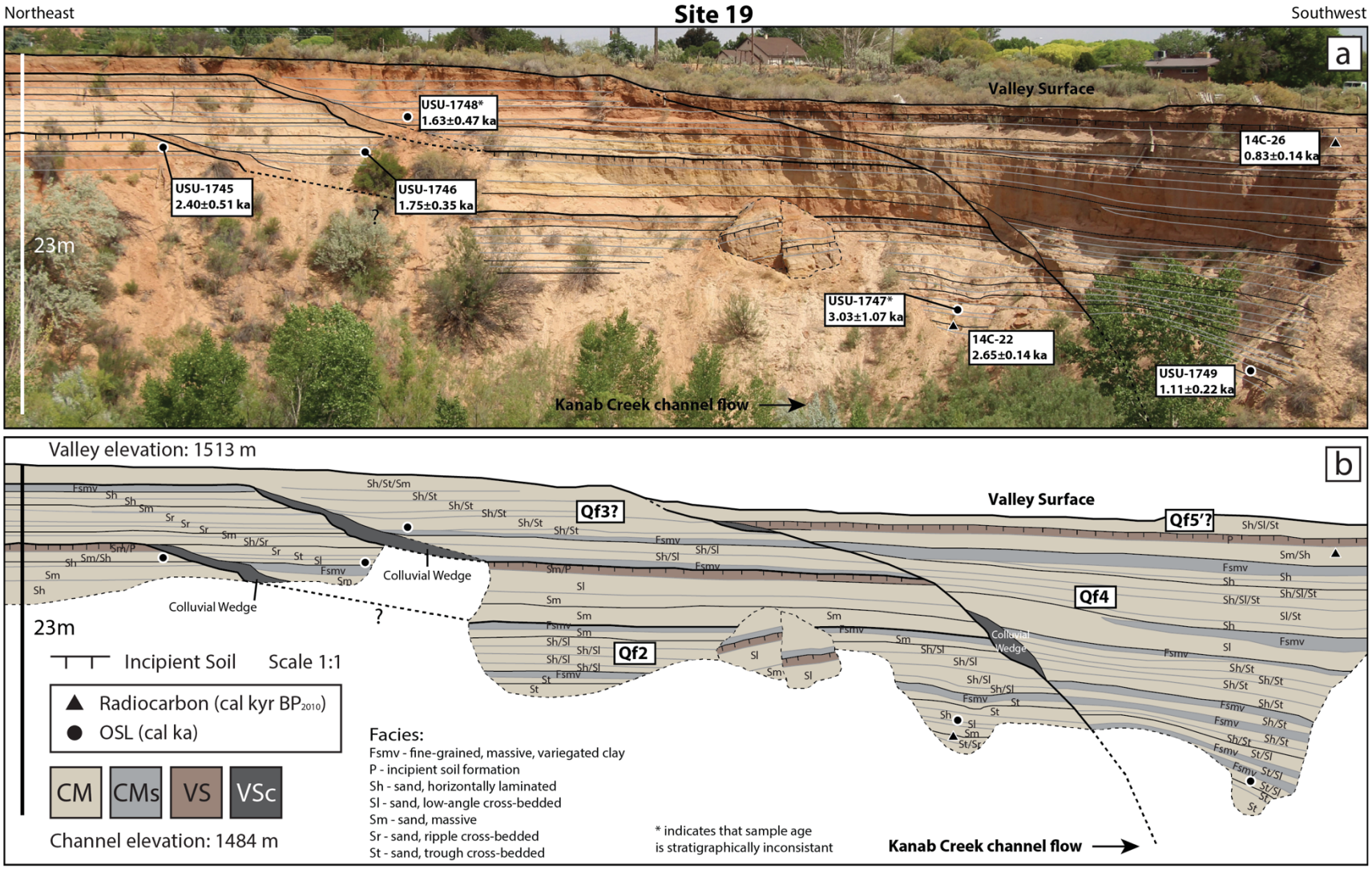

Fig. S19: Site 19 (a) annotated photo with location and age of geochronology samples, and (b) stratigraphic panel and interpreted alluvial fill number.

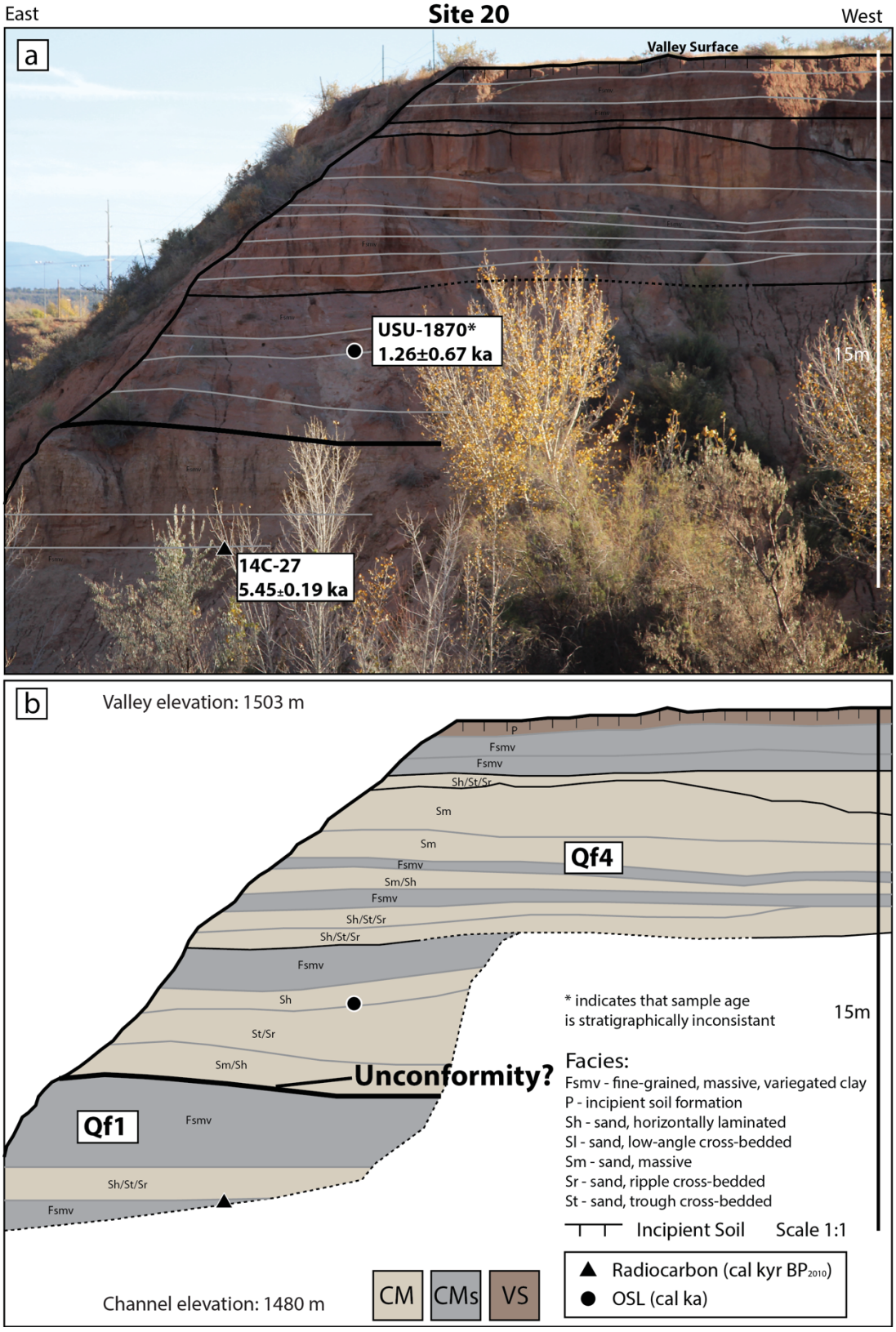

Fig. S20: Site 20 (a) annotated photo with location and age of geochronology samples, and (b) stratigraphic panel and interpreted alluvial fill number.

Site 21

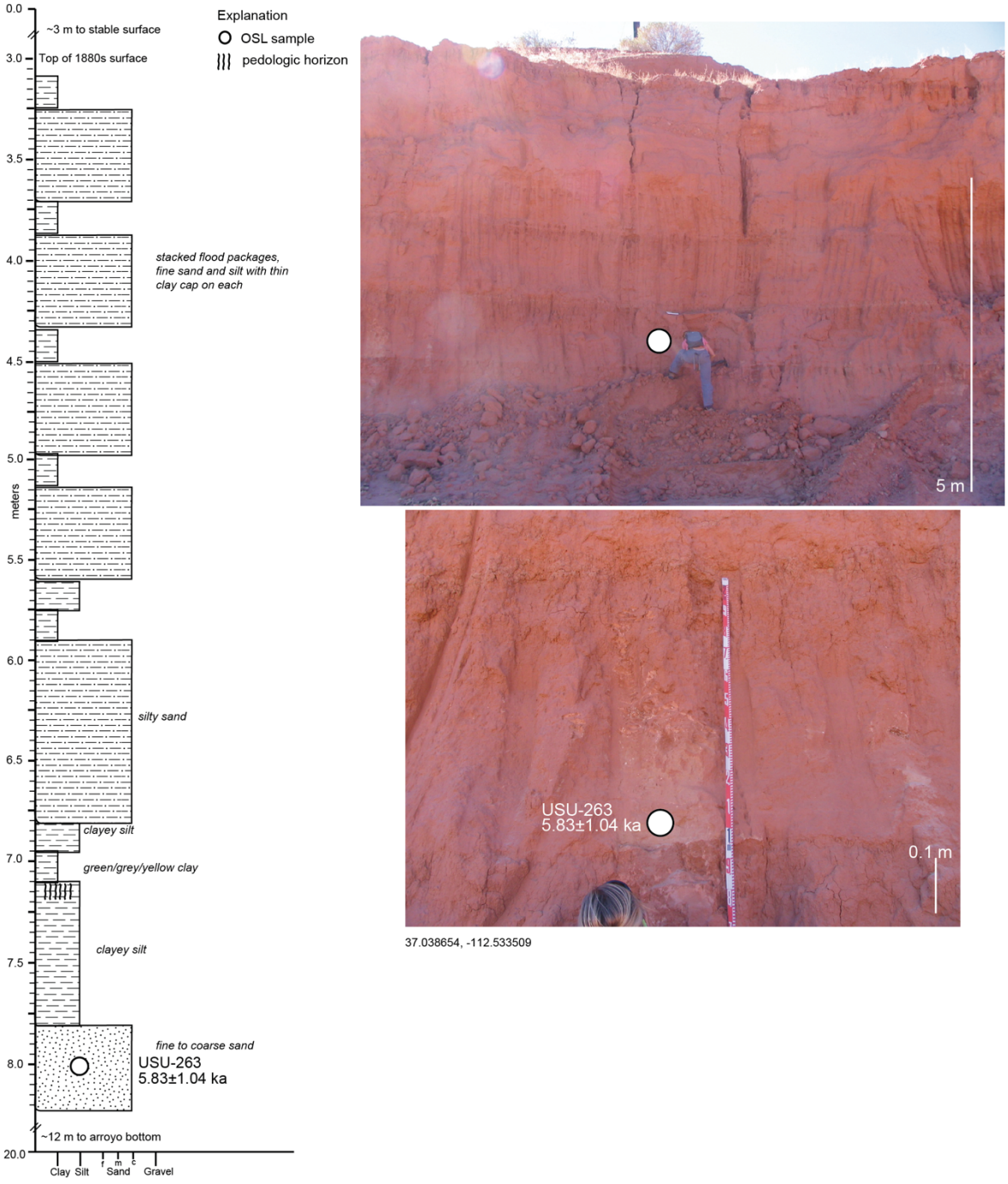

Fig. S21: Site 21 stratigraphic column and annotated photos with location and age of geochronology samples. Site L from Nelson and Rittenour (2014).

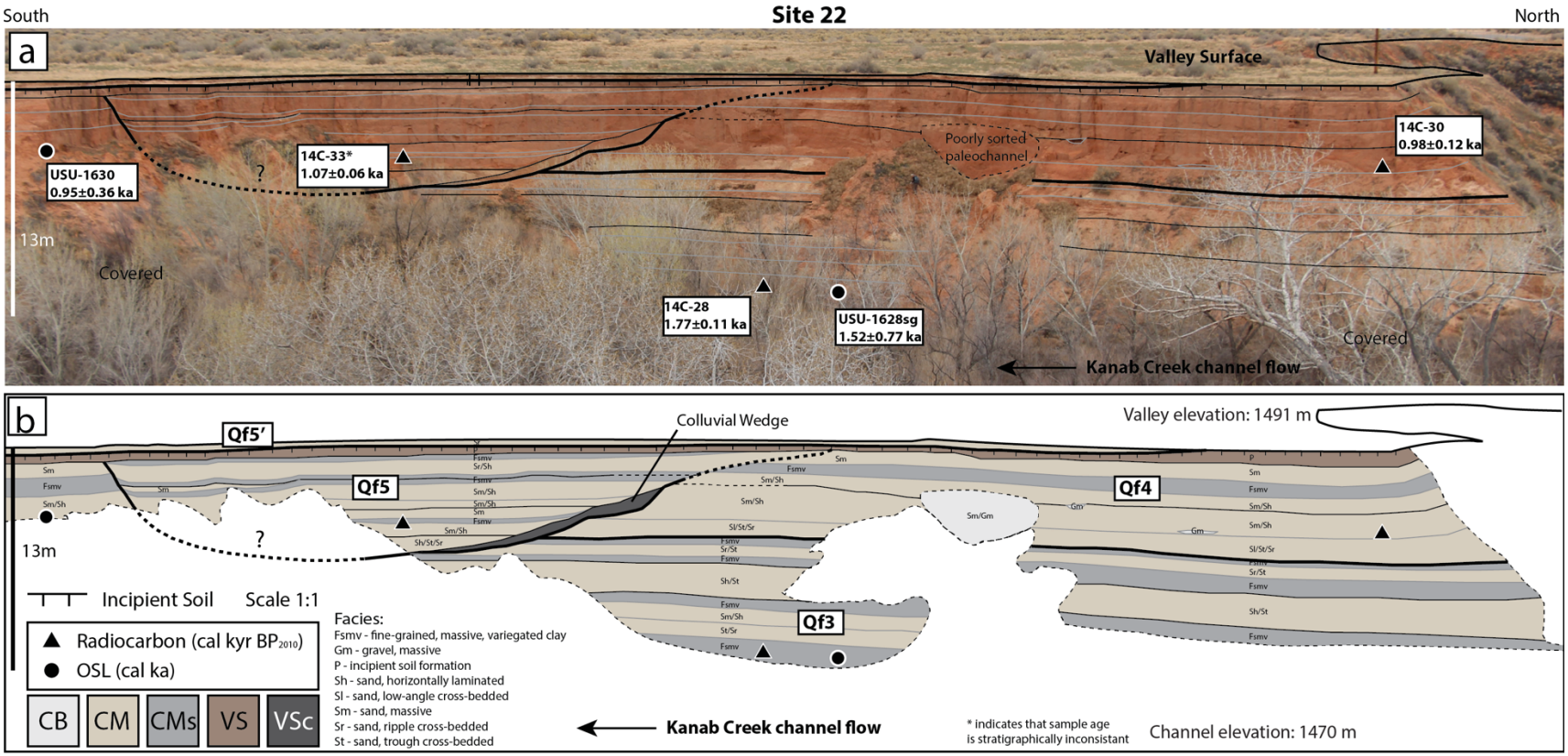

Fig. S22: Site 22 (a) annotated photo with location and age of geochronology samples, and (b) stratigraphic panel and interpreted alluvial fill number.

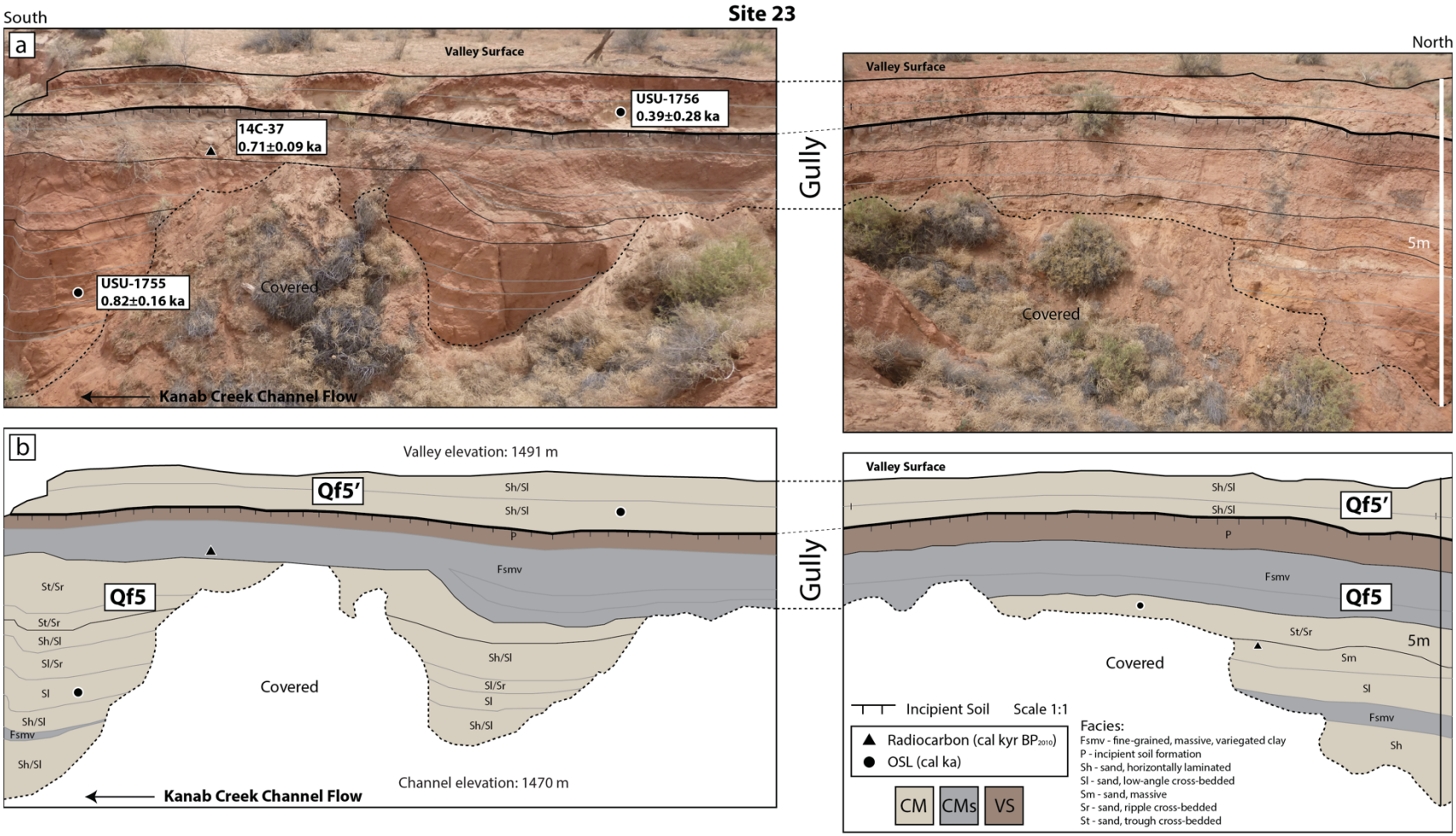

Fig. S23: Site 23 (a) annotated photo with location and age of geochronology samples, and (b) stratigraphic panel and interpreted alluvial fill number.

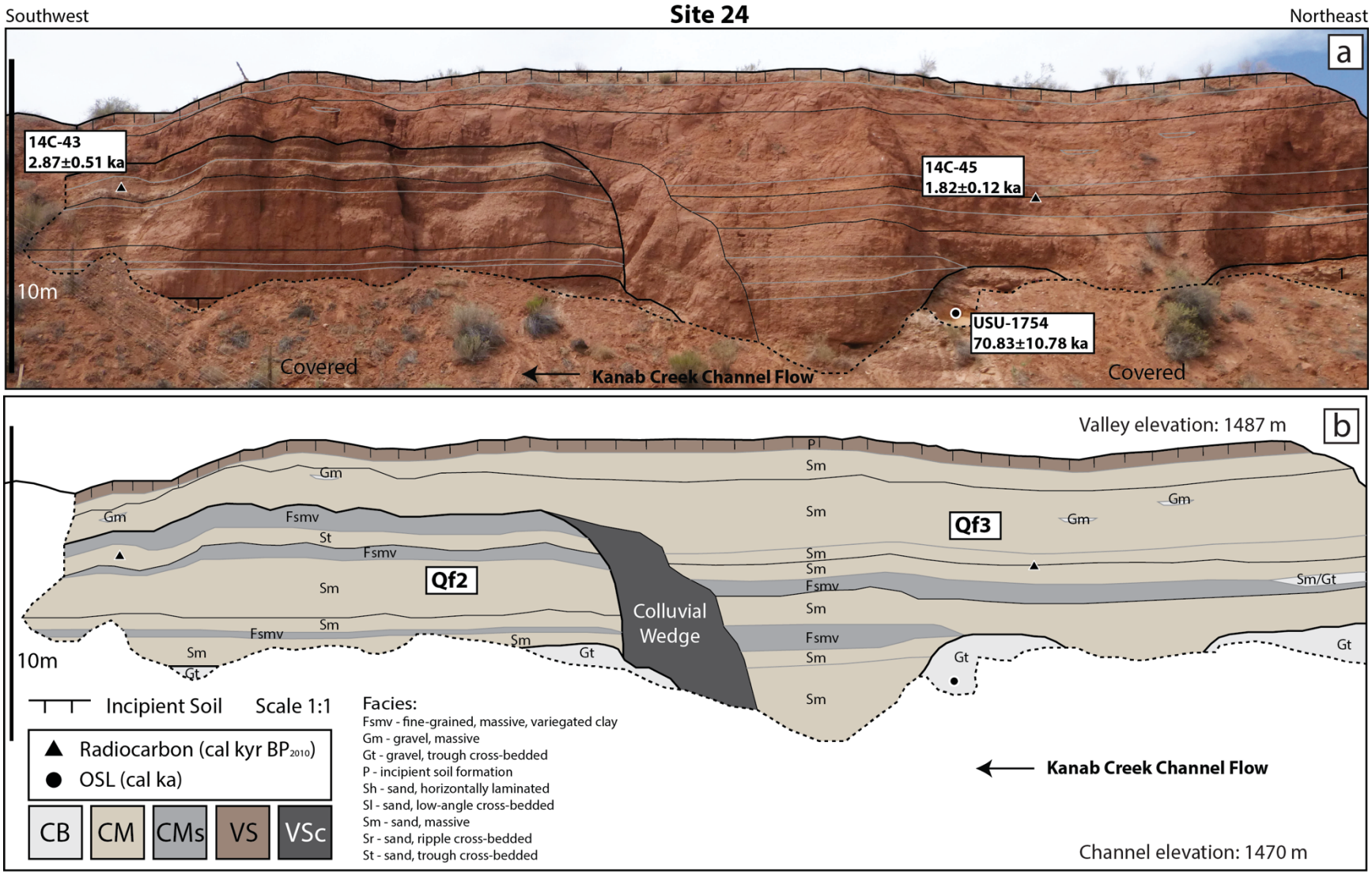

Fig. S24: Site 24 (a) annotated photo with location and age of geochronology samples, and (b) stratigraphic panel and interpreted alluvial fill number.

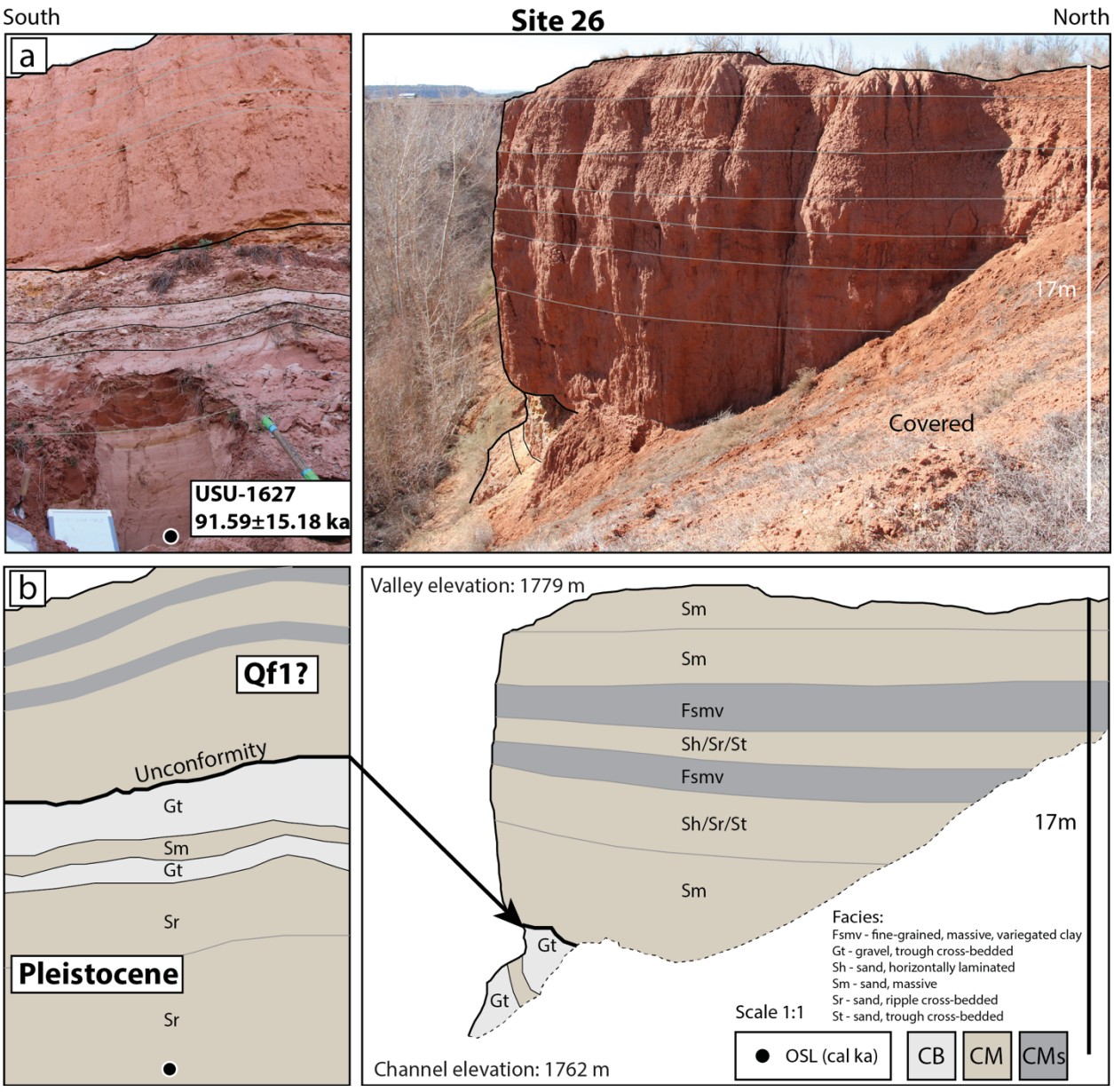

Fig. S25: Site 26 (a) annotated photo with location and age of geochronology samples, and (b) stratigraphic panel and interpreted alluvial fill number.

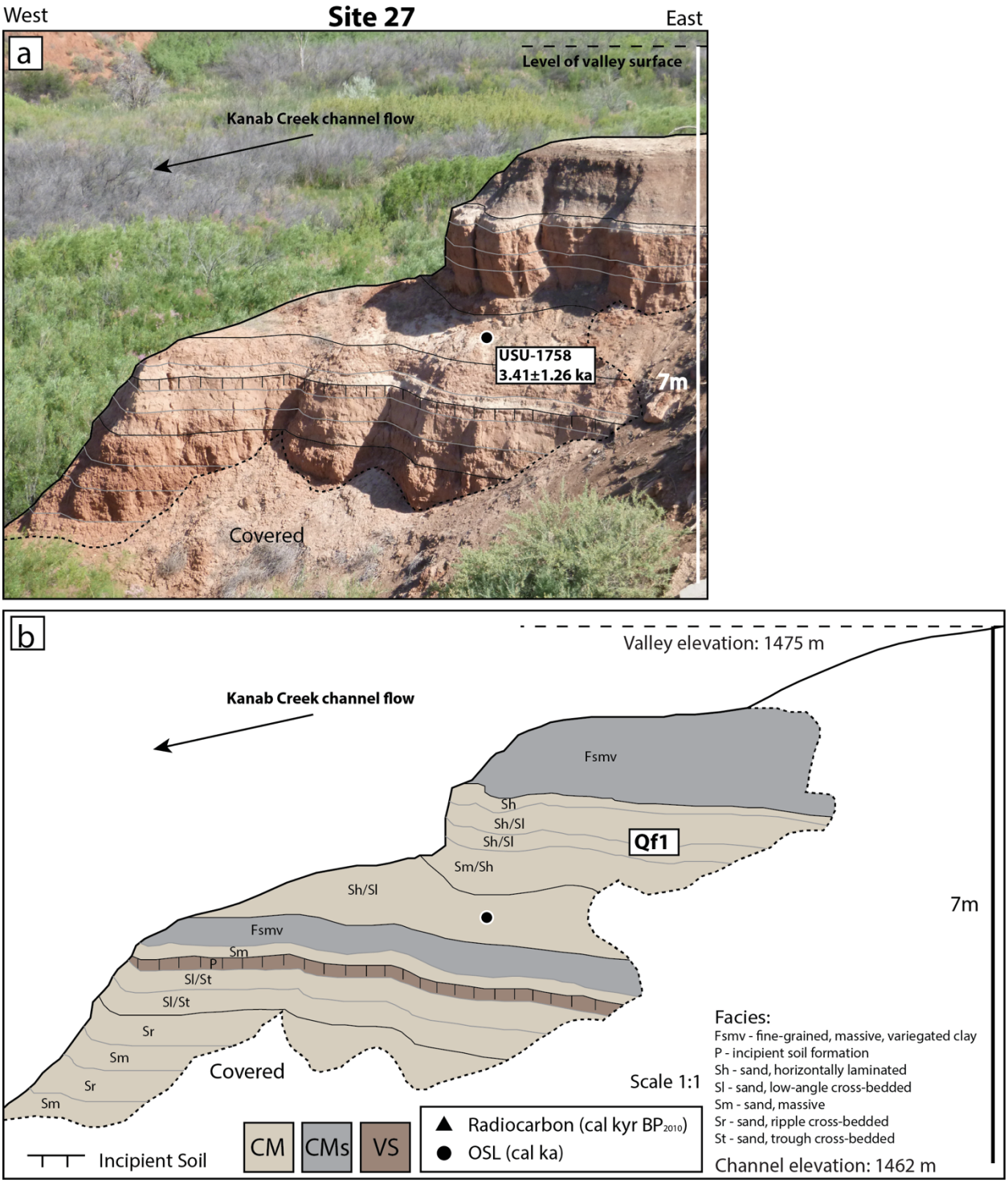

Fig. S26: Site 27 (a) annotated photo with location and age of geochronology samples, and (b) stratigraphic panel and interpreted alluvial fill number.

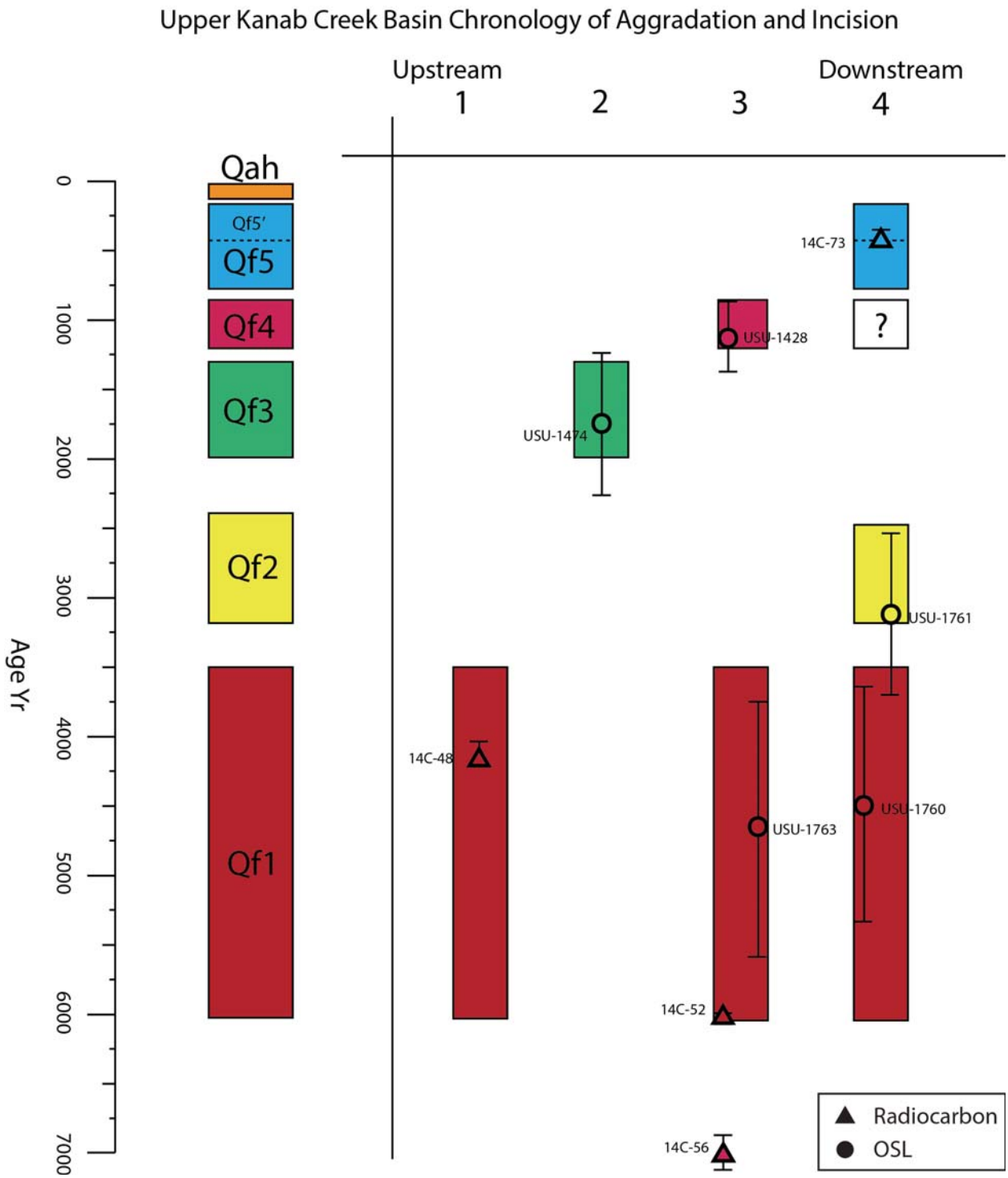

Fig. S27: Chronology of aggradation and inferred episodes of entrenchment in the upper basin reach of Kanab Creek as derived from detailed stratigraphic interpretation, AMS radiocarbon (triangles) and OSL (circles) ages. Orange = Qah historic alluvium, blue = Qf5 fill, pink = Qf4 fill, green = Qf3 fill, yellow = Qf2 fill, and red = Qf1 fill. Colors within radiocarbon triangles and OSL circles indicate stratigraphic package from which samples were collected. An alluvial fill package bracketed by a buttress unconformity and a paleosol at Site 4 was unable to be dated.

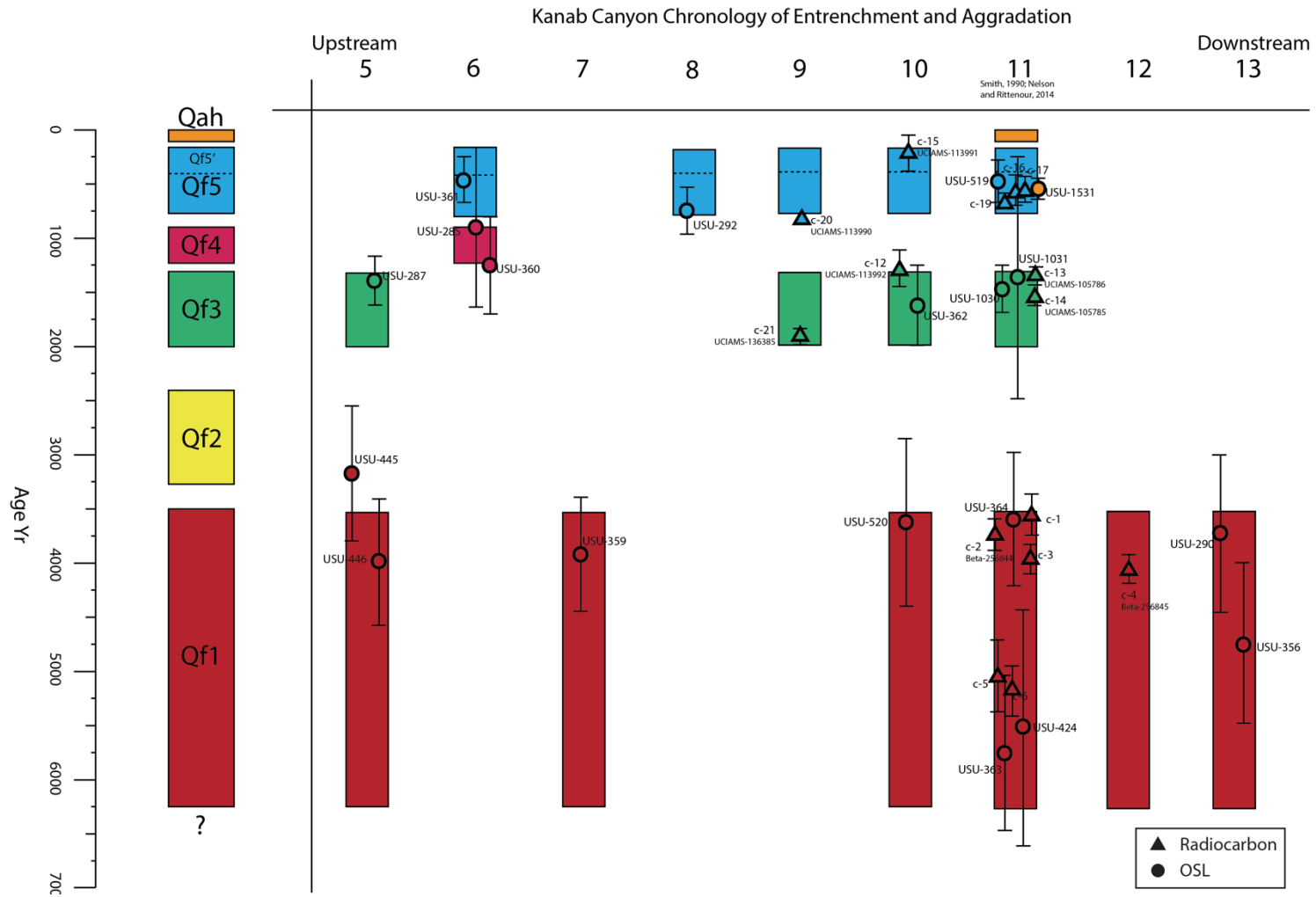

Fig. S28: Chronology of aggradation and inferred episodes of entrenchment in the Canyon reach of Kanab Creek as derived from detailed stratigraphic interpretation, AMS radiocarbon (triangles) and OSL (circles) ages. Orange = Qah historic alluvium, blue = Qf5 fill, pink = Qf4 fill, green = Qf3 fill, yellow = Qf2 fill, and red = Qf1 fill. Colors within radiocarbon triangles and OSL circles

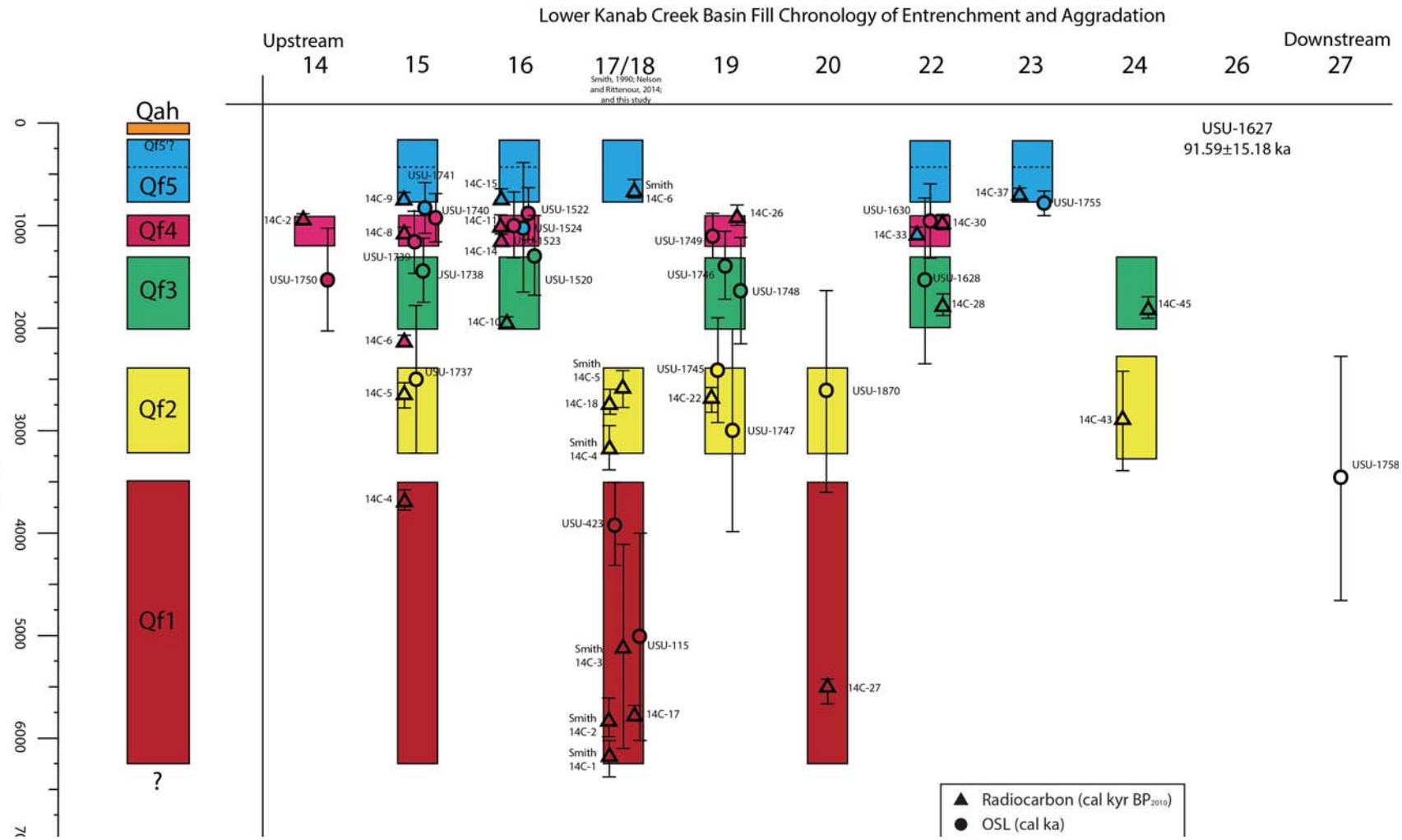

ig. S29: Chronology of aggradation and inferred episodes of entrenchment in the lower basin of Kanab Creek as derived from detailed stratigraphic interpretation, AMS radiocarbon (triangles) and OSL (circles) ages. Orange = Qah historic alluvium, blue = Qf5 fill, pink = Qf4 fill, green = Qf3 fill, yellow = Qf2 fill, and red = Qf1 fill. Colors within radiocarbon triangles and OSL circles

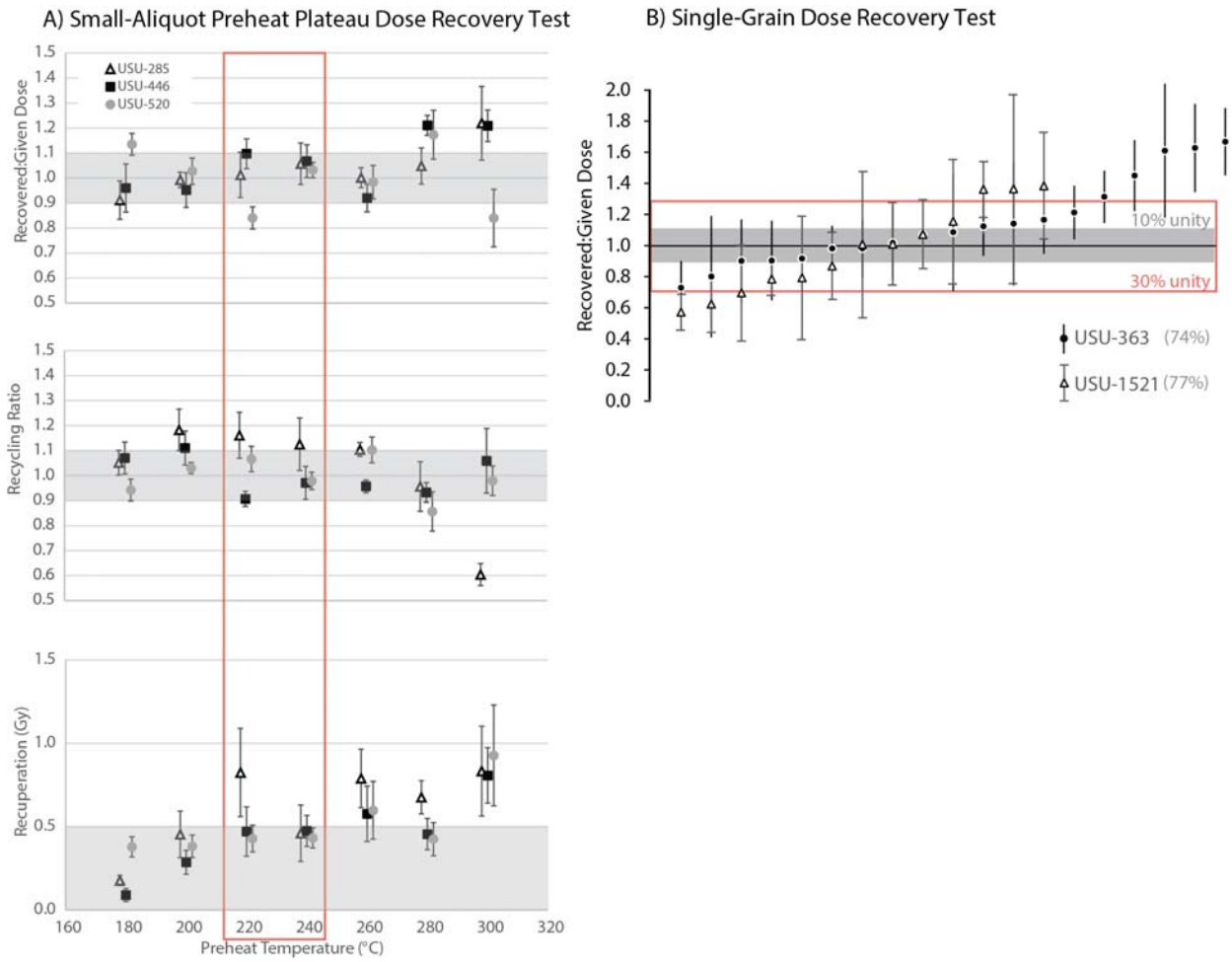

Fig. S30: A) Small-Aliquot Preheat Plateau Dose Recovery test results for USU-285, USU-446, and USU-520, updated from Summa-Nelson and Rittenour (2012). Top is dose recovery results plotted as a ratio of recovered to applied dose for preheat temperatures 180-300ºC. Middle is the recycling ratio results for a repeated beta dose at the beginning and end of the SAR cycle. Bottom is recuperation, or amount of signal measured when no dose is applied, in Gy. Results show 220- 240ºC (orange box) is desirable preheat temperature for Kanab Creek samples given the ratios within 10% of unity (grey region top and middle) and low recuperation (<0.5Gy). B) Single-Grain Dose Recovery Test results, showing grains with recovery ratios up to 10, though 0.7-1.3 is desired range. 240ºC used as preheat temperature for USU-363 test, and 220 ºC used as preheat temperature in USU-1521 test. Orange box indicates grain results that fall within 30% of unity for recovered to given dose ratio. 34% of grains fell within 30% of unity for USU-363, and 26% of grains within 30% of unity for USU-1521.

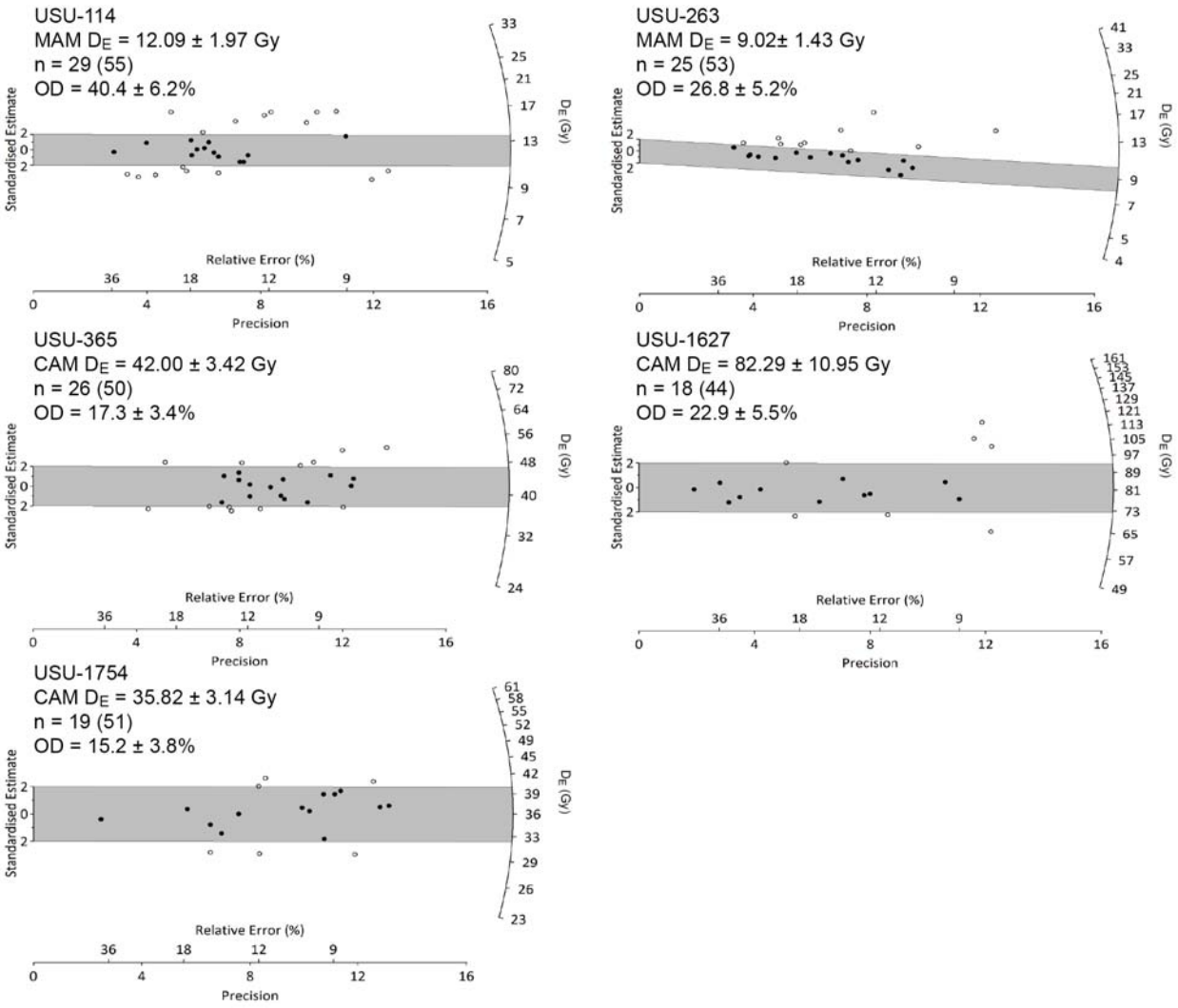

Figure S31: Small-aliquot equivalent-dose (D_E) radial plots for samples USU-114, USU-263, USU-365, USU-1627, USU-1754.

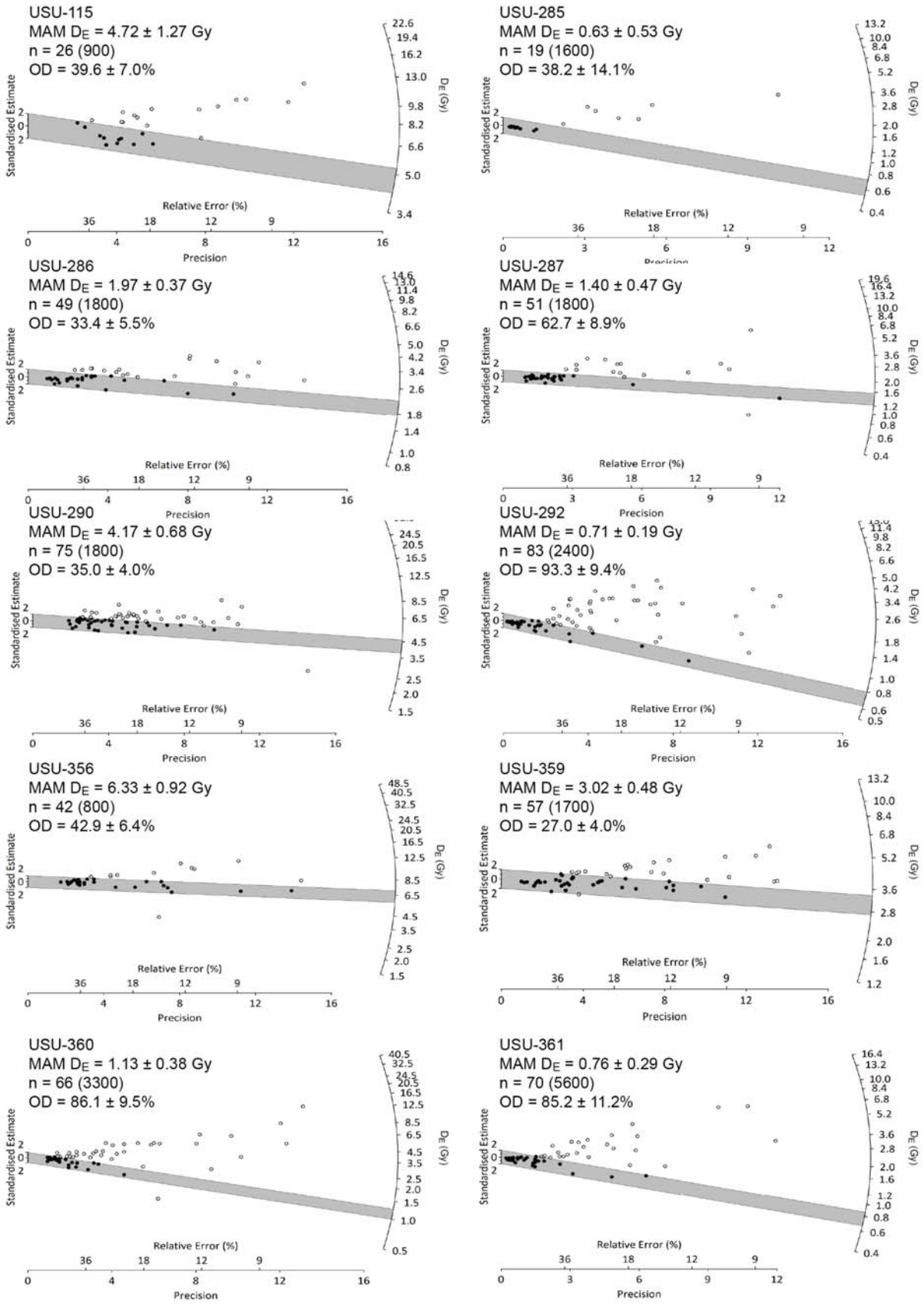

Figure S32: Single-grain equivalent-dose (D_E) radial plots

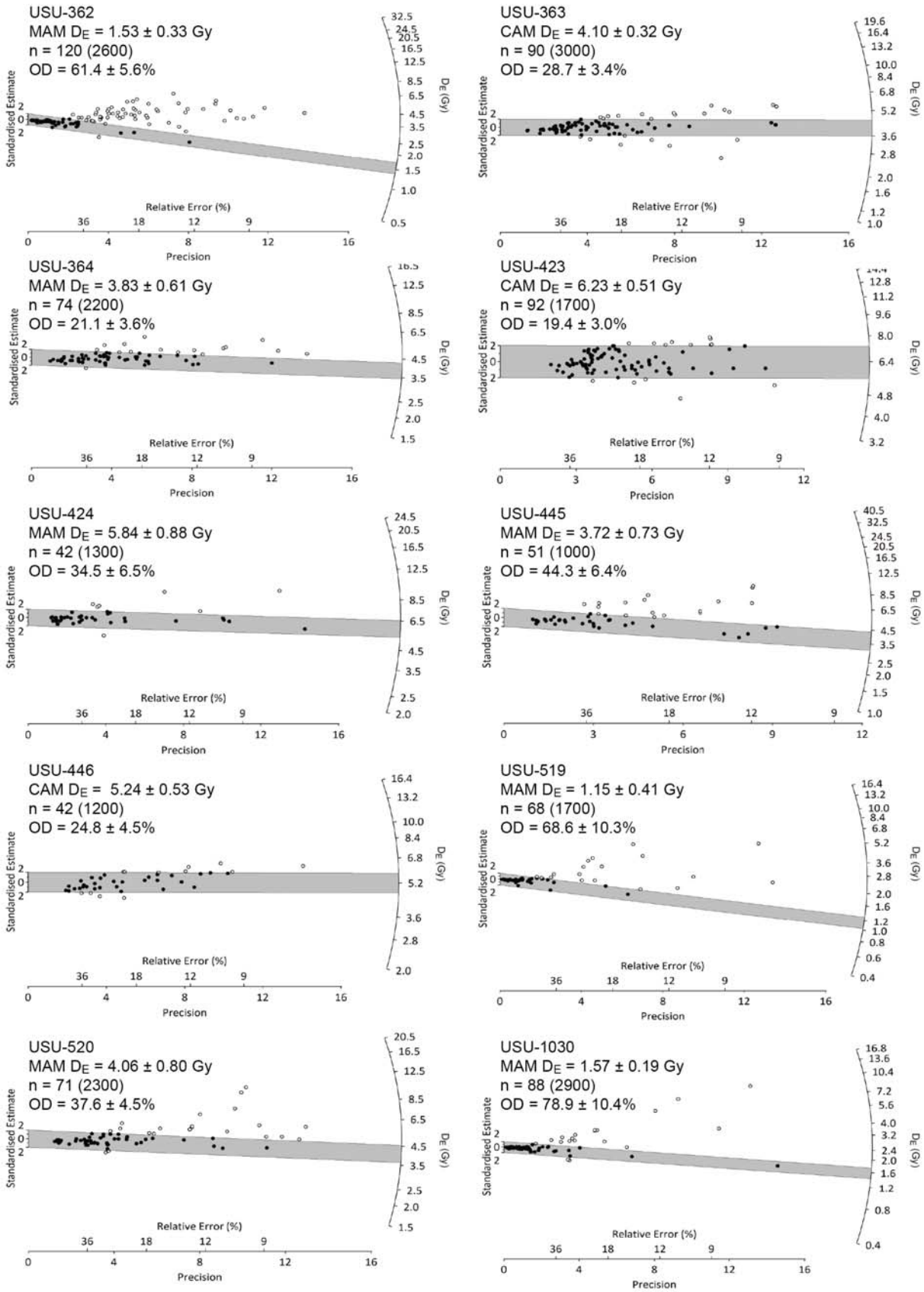

Figure S32: Single-grain equivalent-dose (D_E) radial plots (continued)

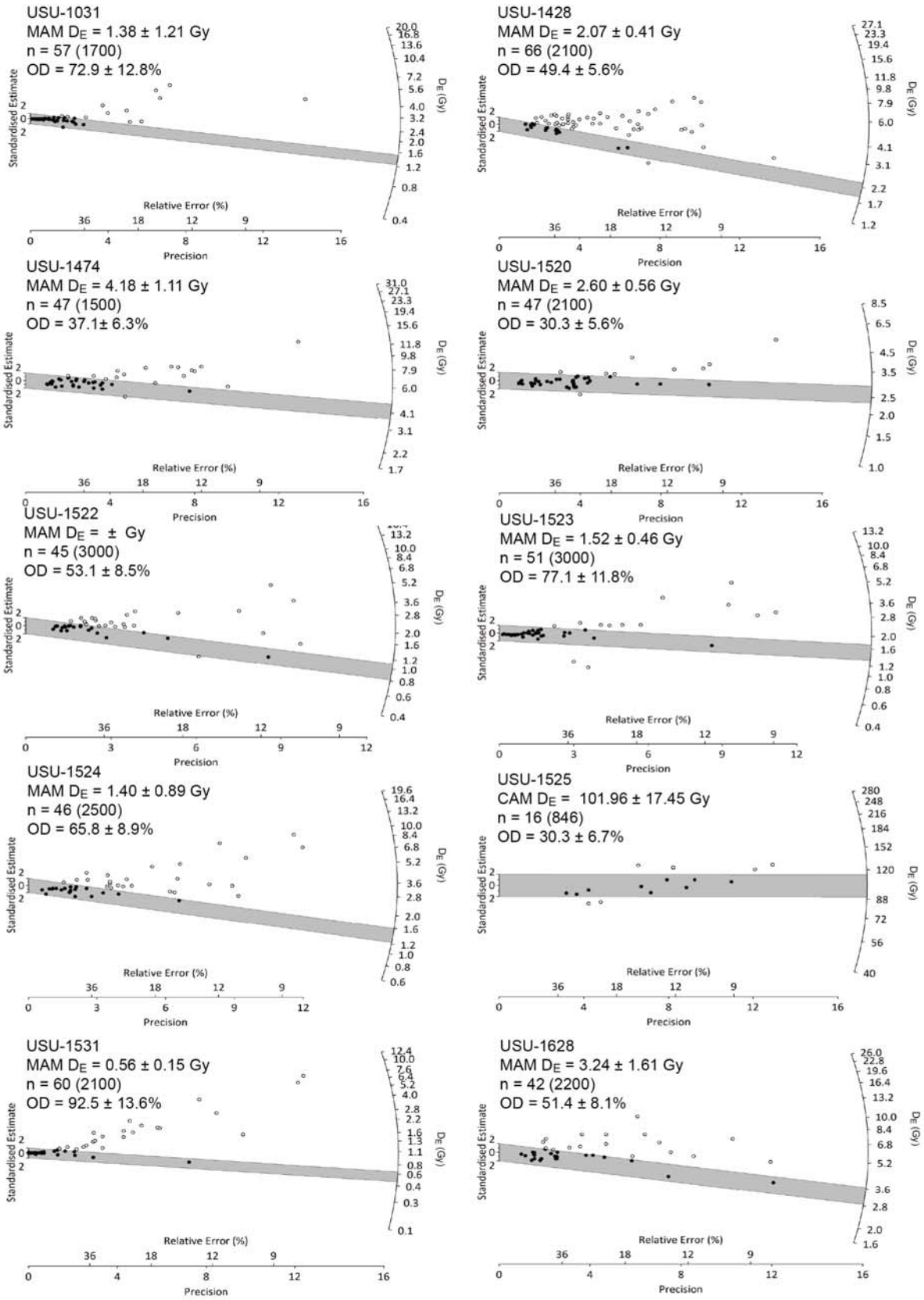

Figure S32: Single-grain equivalent-dose (D_E) radial plots (continued)

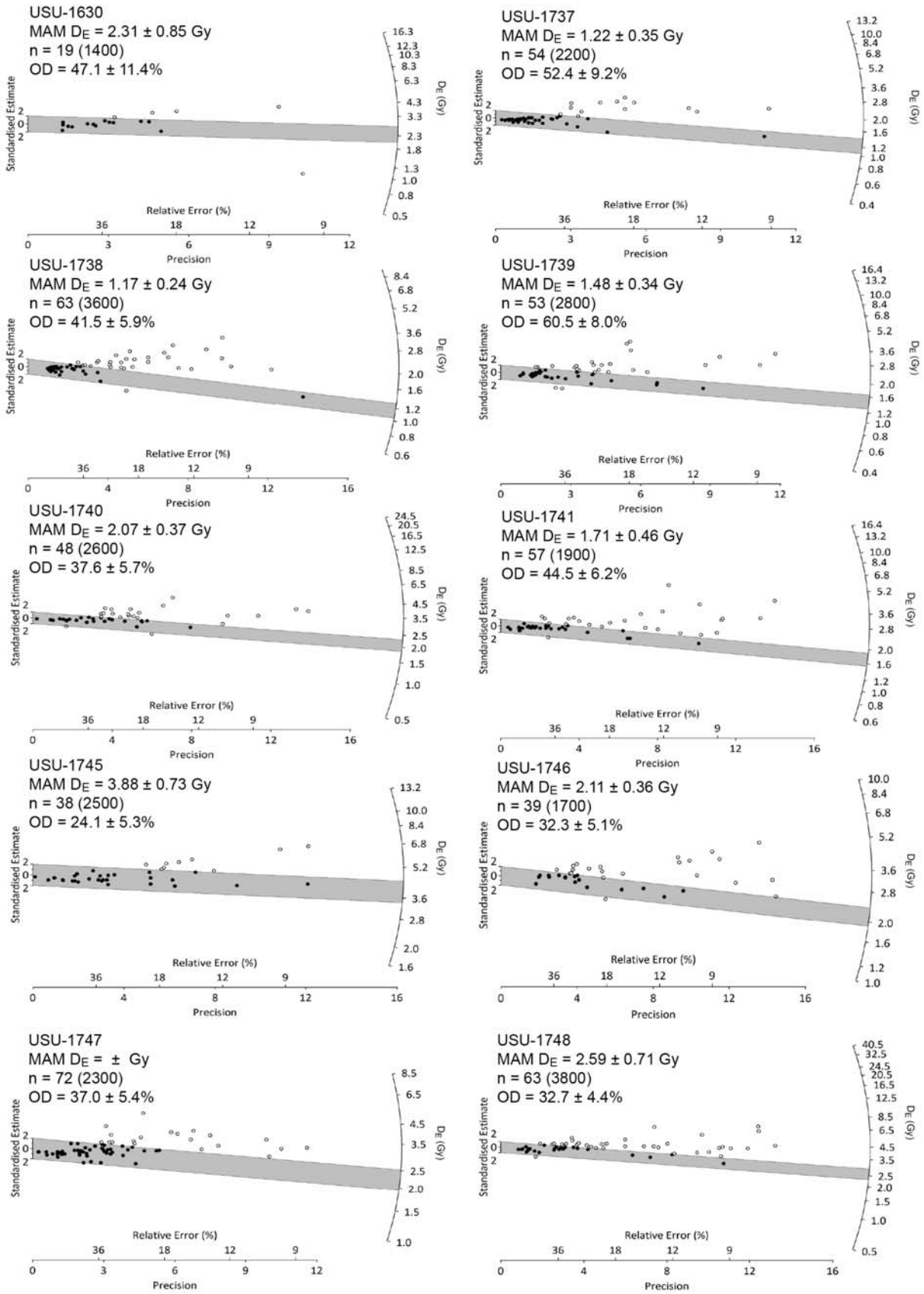

Figure S32: Single-grain equivalent-dose (D_E) radial plots (continued)

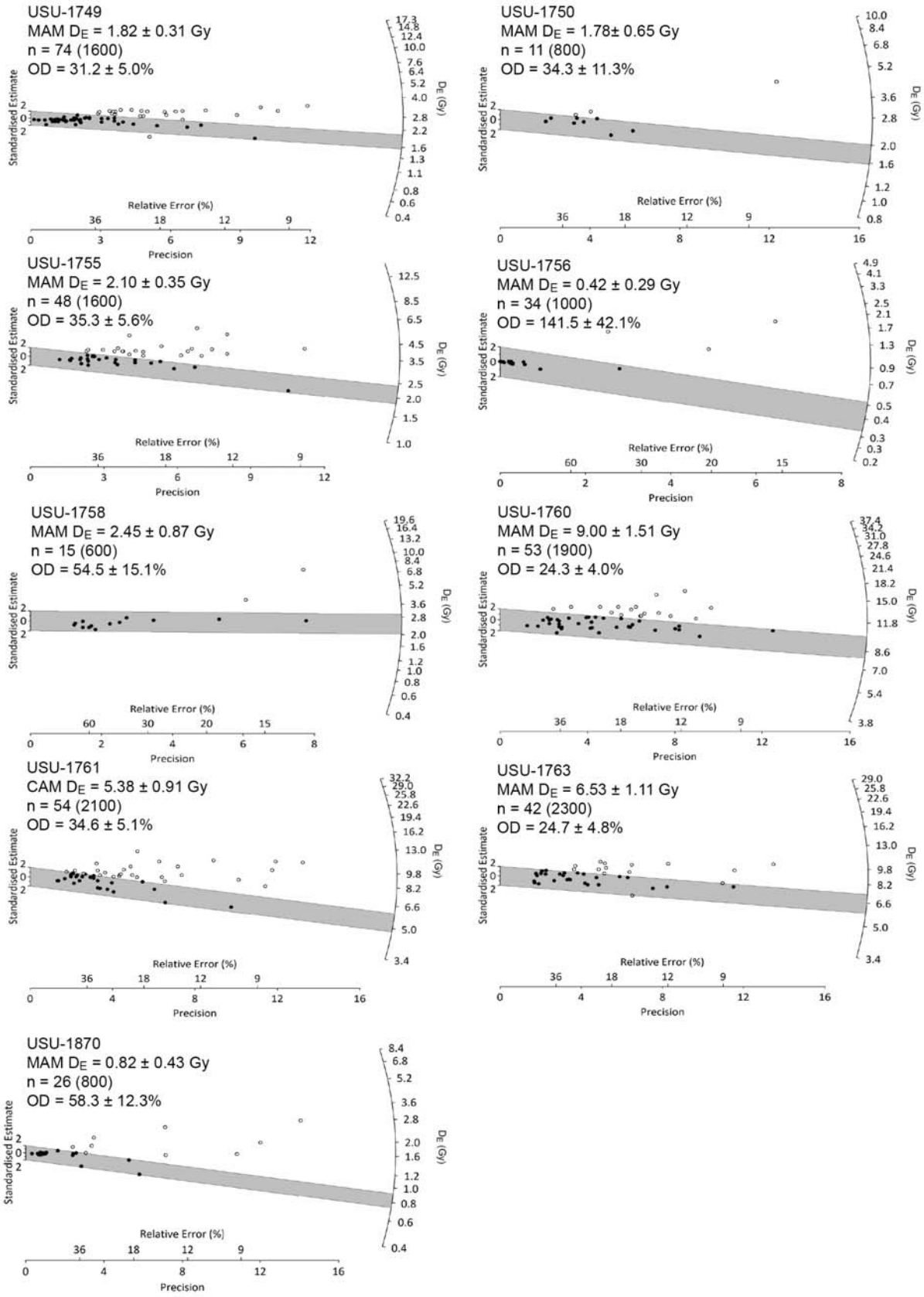

Figure S32: Single-grain equivalent-dose (D_E) radial plots (continued)